

Radiative $H_{1,2}^+W^-Z$ vertices in flavour conserving three Higgs-doublet scenarios

Nabarun Chakrabarty^{*}

*Department of Physics, Siksha Bhavana, Visva-Bharati,
Santiniketan, West Bengal 731235, India*

Indrani Chakraborty[†]

*Department of Physics and Material Science and Engineering,
Jaypee Institute of Information Technology, A-10,
Sector-62, Noida 201307, Uttar Pradesh, India*

Abstract

A detailed calculation of the radiatively induced $H_{1,2}^+W^-Z$ vertices is carried out in the context of flavour conserving three Higgs doublet models (3HDMs). The Type-II, lepton specific and democratic versions of the 3HDM are chosen as representative cases and the *alignment limit* is adopted. We arrange the amplitudes in UV-finite and gauge-invariant subsets for a sharper understanding of the underlying one-loop structure. Factoring-in various theoretical constraints and the ones from the $h \rightarrow \gamma\gamma$ signal strength and the $B \rightarrow X_s\gamma$ branching ratio, we compute the relevant form factors and compare them among the various 3HDM types taken. The results also indicate a sizeable increment ($\sim 100\%$) over the corresponding form factors in 2HDMs. In addition, we probe the $H_{1,2}^+W^-Z$ vertices at the 14 TeV LHC using vector boson fusion (VBF). It is seen that production of H_1^+ via VBF and the subsequent $H_1^+ \rightarrow H_2^+H_2/A_2$ decays can have $\sigma \times \text{BR}$ in the $\mathcal{O}(0.1 \text{ fb})$ ball park. Therefore, such a cascade can shed light on the strength of the $H_1^+W^-Z$ interaction and confirm the presence of two charged scalars thereby acting as a smoking gun signal of a 3HDM.

^{*}Electronic address: nabarun.chakrabarty@visva-bharati.ac.in

[†]Electronic address: indrani.chakraborty@jiit.ac.in

I. INTRODUCTION

The discovery of the Higgs boson with a mass around 125 GeV at the Large Hadron Collider (LHC) [1, 2] has completed the particle content of Standard Model (SM). While the SM minimally accounts for electroweak symmetry breaking (EWSB) and fermion mass generation, it leaves many fundamental questions unanswered on both theoretical and experimental fronts. This renders the SM far from being a complete theory thereby motivating extensions Beyond the SM (BSM). However, the LHC has been consistently reporting that the interaction strengths of the scalar with the SM fermions and gauge bosons are in good agreement with the corresponding SM predictions. Such results, along with a host of null outcomes pertaining to direct searches of additional degrees freedom, have collectively pushed a plethora of BSM scenarios at bay.

That said, extended scalar sectors—particularly those with additional Higgs doublets—provide simplistic framework to address several of these shortcomings. Multi-Higgs doublet frameworks can be motivated from several perspectives. First, there is no restriction on the number of scalar doublets from fundamental principles, especially when the ρ -parameter is maintained at unity at the tree level in the presence of $SU(2)_L$ scalar doublets. Secondly, such frameworks shut off flavour changing neutral currents (FCNC), predict additional CP-violation through the scalar potential that can eventually explain the observed matter-antimatter imbalance. Thirdly, the same setups can accommodate an *alignment limit* wherein the interactions of one of the CP-even scalars, identified with the discovered boson, become identical to the corresponding SM ones. Though many interactions involving the non-standard scalars and gauge bosons vanish at an exact alignment, such scalars can still be probed at particle colliders primarily through their fermionic interactions, modulo the restrictions from direct search.

The most minimal and also the most widely studied multi-Higgs doublet setup is the two-Higgs doublet model (2HDM) [3–8] and it can emerge in diverse theoretical contexts such as supersymmetry, axion models, flavor symmetries, and grand unification. FCNCs in this case can be annulled by imposing a single \mathbb{Z}_2 symmetry. A 2HDM is in fact the smallest non-trivial $SU(2)_L$ multiplet to predict a singly charged Higgs H^+ . An H^+ can be searched at the LHC through its fermionic interactions. While an $H^+ \rightarrow t\bar{b}$ mode is useful to look for an heavy H^+ , an $H^+ \rightarrow \tau\nu_\tau$ channel becomes more suited to an appropriately light one. However, heavy QCD backgrounds can limit the observability of such modes thereby advocating the need to look at other channels, the bosonic decays $H^+ \rightarrow W^+ h$, $W^+ Z$, $W^- \gamma$, for instance. That said, the last two of the aforementioned modes are *prima facie* more intriguing since they arise only at one-loop in multi-Higgs doublet models [9].

The absence of the $H^+W^-Z(\gamma)$ coupling at the tree level is an artefact of the isospin symmetry of the kinetic terms of the Higgs sector. Since both these characteristics are, in general, broken radiatively through quantum effects from other sectors that do not respect the custodial invariance, these vertices are potentially induced at the one-loop level. It is therefore established that the strength of the $H^+W^-Z(\gamma)$ interaction quantifies the extent of custodial symmetry breaking in the embedding model. Moreover, the fact that a radiatively induced $H^+W^-Z(\gamma)$ vertex carries a momentum-dependence distinguishes a multi-Higgs doublet setup from one featuring scalar triplets (since the tree-level H^+W^-Z interaction in case of the latter does not carry any momentum-dependence). The $H^+W^-Z(\gamma)$ interaction at one-loop has been studied in various versions of the 2HDM in [10–14] and in a scenario comprising two scalar doublets and a scalar iso-doublet color octet in [15].

The next minimal multi-Higgs doublet framework is the three-Higgs doublet model (3HDM). Various aspects of the 3HDMs have also been studied in the recent past, a partial list of which is [16? –45]. In this work, we study in detail the $H_1^+W^-Z$ and $H_2^+W^-Z$ vertices at one-loop in the context of flavour-conserving 3HDMs of Type-II, Type-X and Type-Z¹. Discrete symmetry-breaking quadratic terms are allowed for phenomenological reasons and an exact alignment is demanded. It must be mentioned here that while [46] investigated the $H^+W^-Z(\gamma)$ interaction for the three Higgs doublet scenario, of the doublets was *inert* and therefore the aforementioned interaction was forbidden for the inert charged scalar. The main features of the present study are outlined below.

- We adopt a non-linear gauge where the unphysical G^+W^-Z vertex disappears. This makes a check of gauge invariance easier using Ward identity. Further, we divide the one-loop amplitudes into UV-finite and gauge invariant subsets.
- Given the existing literature on 3HDM, we refrain from performing an exhaustive parameter space scan. We therefore adopt a simplified approach by adhering to the alignment limit and enforcing additional relations involving model parameters to satisfy electroweak precision constraints.
- We look for possible (anti)correlations between the form factors corresponding to H_1^+ and H_2^+ . We also look to discern a possible enhancement of the form factors over 2HDM.
- The $H_{1,2}^+W^-Z$ interaction is probed at the 14 TeV LHC through vector boson fusion (VBF) in this study. Further the decays $H_1^+ \rightarrow H_2^+H_2$, H^+A_2 are investigated that can confirm the

¹ The rationale behind picking the aforesaid variants is relegated to the following sections

presence of two charged scalars. Therefore such a cascade can be used a smoking gun signal of a 3HDM.

This study is organised as follows. We review the flavour-conserving 3HDM types under a $\mathbb{Z}_2 \times \mathbb{Z}'_2 \times \mathbb{Z}''_2$ symmetry in section II. In section III, the one-loop form factors are detailed and their UV-finiteness and gauge invariance are demonstrated. The relevant constraints are discussed in section IV. Numerical estimation of the form factors is carried out in section V and collider signatures are elucidated in section VI. We conclude in section VII.

II. FLAVOUR CONSERVING THREE HIGGS DOUBLET MODELS

A. Scalar sector

We introduce three scalar doublets ϕ_1, ϕ_2 and ϕ_3 that are parametrized as :

$$\Phi_j = \begin{pmatrix} \omega_j^+ \\ \frac{1}{\sqrt{2}}(v_j + h_j + iz_j) \end{pmatrix}, \quad j = 1, 2, 3. \quad (1)$$

Here, v_1, v_2 and v_3 are the three vacuum expectation values (VEVs) satisfying $v_1^2 + v_2^2 + v_3^2 = v^2$ with $v = 246$ GeV, and, ω_j^+, h_j and z_j respectively denote the charged, CP-even and CP-odd components. One additionally defines $\tan \beta = \frac{v_2}{v_1}$ and $\tan \gamma = \frac{\sqrt{v_1^2 + v_2^2}}{v_3}$. Thus, $v_1 = v \cos \beta \sin \gamma$, $v_2 = v \sin \beta \sin \gamma$, $v_3 = v \cos \gamma$. Further, aiming to suppress FCNCs, the framework is endowed with a $\mathbb{Z}_2 \times \mathbb{Z}'_2 \times \mathbb{Z}''_2$ symmetry under which Φ_1, Φ_2 and Φ_3 respectively are assigned the charges $(+, +, -)$, $(+, -, +)$ and $(-, +, +)$. The most general scalar potential consistent with the SM and discrete symmetries is therefore

$$\begin{aligned} V = & m_{11}^2 \Phi_1^\dagger \Phi_1 + m_{22}^2 \Phi_2^\dagger \Phi_2 + m_{33}^2 \Phi_3^\dagger \Phi_3 \\ & - [m_{12}^2 \Phi_1^\dagger \Phi_2 + m_{13}^2 \Phi_1^\dagger \Phi_3 + m_{23}^2 \Phi_2^\dagger \Phi_3 + \text{h.c.}] \\ & + \frac{1}{2} \lambda_1 (\Phi_1^\dagger \Phi_1)^2 + \frac{1}{2} \lambda_2 (\Phi_2^\dagger \Phi_2)^2 + \frac{1}{2} \lambda_3 (\Phi_3^\dagger \Phi_3)^2 \\ & + \lambda_{12} (\Phi_1^\dagger \Phi_1)(\Phi_2^\dagger \Phi_2) + \lambda_{13} (\Phi_1^\dagger \Phi_1)(\Phi_3^\dagger \Phi_3) + \lambda_{23} (\Phi_2^\dagger \Phi_2)(\Phi_3^\dagger \Phi_3) \\ & + \lambda'_{12} (\Phi_1^\dagger \Phi_2)(\Phi_2^\dagger \Phi_1) + \lambda'_{13} (\Phi_1^\dagger \Phi_3)(\Phi_3^\dagger \Phi_1) + \lambda'_{23} (\Phi_2^\dagger \Phi_3)(\Phi_3^\dagger \Phi_2) \\ & + \frac{1}{2} [\lambda''_{12} (\Phi_1^\dagger \Phi_2)^2 + \lambda''_{13} (\Phi_1^\dagger \Phi_3)^2 + \lambda''_{23} (\Phi_2^\dagger \Phi_3)^2 + \text{h.c.}]. \end{aligned} \quad (2)$$

All parameters above are chosen real and dimension-2 terms are included in Eq.2 that break the discrete symmetry *softly*. The physical mass spectrum is spanned by the charged scalars H_1^+ and

H_2^+ , the CP-odd neutral scalars A_1 and A_2 , and, the CP-even neutral scalars h, H_1 and H_2 . Of these, h is chosen to be the observed Higgs.

The tadpole conditions $\left(\frac{\partial V}{\partial h_i}\right)_{(v_1, v_2, v_3)} = 0$, for $i = 1, 2, 3$, lead to

$$\begin{aligned} m_{11}^2 &= \frac{1}{v_1} \left(m_{12}^2 v_2 + m_{13}^2 v_3 - \frac{\lambda_1}{2} v_1^3 - \frac{\lambda_{12}}{2} v_1 v_2^2 - \frac{\lambda'_{12}}{2} v_1 v_2^2 - \frac{\lambda''_{12}}{2} v_1 v_2^2 \right. \\ &\quad \left. - \frac{\lambda_{13}}{2} v_1 v_3^2 - \frac{\lambda'_{13}}{2} v_1 v_3^2 - \frac{\lambda''_{13}}{2} v_1 v_3^2 \right), \end{aligned} \quad (3a)$$

$$\begin{aligned} m_{22}^2 &= \frac{1}{v_2} \left(m_{12}^2 v_1 + m_{23}^2 v_3 - \frac{\lambda_2}{2} v_2^3 - \frac{\lambda_{12}}{2} v_2 v_1^2 - \frac{\lambda'_{12}}{2} v_2 v_1^2 - \frac{\lambda''_{12}}{2} v_2 v_1^2 \right. \\ &\quad \left. - \frac{\lambda_{23}}{2} v_2 v_3^2 - \frac{\lambda'_{23}}{2} v_2 v_3^2 - \frac{\lambda''_{23}}{2} v_2 v_3^2 \right), \end{aligned} \quad (3b)$$

$$\begin{aligned} m_{33}^2 &= \frac{1}{v_3} \left(m_{13}^2 v_1 + m_{23}^2 v_2 - \frac{\lambda_3}{2} v_3^3 - \frac{\lambda_{13}}{2} v_3 v_1^2 - \frac{\lambda'_{13}}{2} v_3 v_1^2 - \frac{\lambda''_{13}}{2} v_3 v_1^2 \right. \\ &\quad \left. - \frac{\lambda_{23}}{2} v_3 v_2^2 - \frac{\lambda'_{23}}{2} v_3 v_2^2 - \frac{\lambda''_{23}}{2} v_3 v_2^2 \right). \end{aligned} \quad (3c)$$

The mass terms can subsequently be expressed as

$$V \supset \frac{1}{2} \begin{pmatrix} h_1 & h_2 & h_3 \end{pmatrix} \mathcal{M}_{\text{even}}^2 \begin{pmatrix} h_1 \\ h_2 \\ h_3 \end{pmatrix} + \frac{1}{2} \begin{pmatrix} z_1 & z_2 & z_3 \end{pmatrix} \mathcal{M}_{\text{odd}}^2 \begin{pmatrix} z_1 \\ z_2 \\ z_3 \end{pmatrix} + \begin{pmatrix} \omega_1^- & \omega_2^- & \omega_3^- \end{pmatrix} \mathcal{M}_{\text{ch}}^2 \begin{pmatrix} \omega_1^+ \\ \omega_2^+ \\ \omega_3^+ \end{pmatrix} \quad (4)$$

The mass matrices in the gauge basis, i.e., $\mathcal{M}_{\text{even}}^2$, $\mathcal{M}_{\text{odd}}^2$ and $\mathcal{M}_{\text{ch}}^2$ are given in the Appendix. These matrices can be diagonalised using appropriate unitary transformations connecting the gauge and physical bases. Therefore, one writes in the lines of [40, 47]

$$\begin{pmatrix} h \\ H_1 \\ H_2 \end{pmatrix} = \begin{pmatrix} 1 & 0 & 0 \\ 0 & c_{\alpha_3} & s_{\alpha_3} \\ 0 & -s_{\alpha_3} & c_{\alpha_3} \end{pmatrix} \begin{pmatrix} c_{\alpha_2} & 0 & s_{\alpha_2} \\ 0 & 1 & 0 \\ -s_{\alpha_2} & 0 & c_{\alpha_2} \end{pmatrix} \begin{pmatrix} c_{\alpha_1} & s_{\alpha_1} & 0 \\ -s_{\alpha_1} & c_{\alpha_1} & 0 \\ 0 & 0 & 1 \end{pmatrix} \begin{pmatrix} h_1 \\ h_2 \\ h_3 \end{pmatrix}, \quad (5a)$$

$$\begin{pmatrix} G^0 \\ A_1 \\ A_2 \end{pmatrix} = \begin{pmatrix} 1 & 0 & 0 \\ 0 & c_{\delta_1} & -s_{\delta_1} \\ 0 & s_{\delta_1} & c_{\delta_1} \end{pmatrix} \begin{pmatrix} s_{\gamma} & 0 & c_{\gamma} \\ 0 & 1 & 0 \\ -c_{\gamma} & 0 & s_{\gamma} \end{pmatrix} \begin{pmatrix} c_{\beta} & s_{\beta} & 0 \\ -s_{\beta} & c_{\beta} & 0 \\ 0 & 0 & 1 \end{pmatrix} \begin{pmatrix} z_1 \\ z_2 \\ z_3 \end{pmatrix}, \quad (5b)$$

$$\begin{pmatrix} G^+ \\ H_1^+ \\ H_2^+ \end{pmatrix} = \begin{pmatrix} 1 & 0 & 0 \\ 0 & c_{\delta_2} & -s_{\delta_2} \\ 0 & s_{\delta_2} & c_{\delta_2} \end{pmatrix} \begin{pmatrix} s_{\gamma} & 0 & c_{\gamma} \\ 0 & 1 & 0 \\ -c_{\gamma} & 0 & s_{\gamma} \end{pmatrix} \begin{pmatrix} c_{\beta} & s_{\beta} & 0 \\ -s_{\beta} & c_{\beta} & 0 \\ 0 & 0 & 1 \end{pmatrix} \begin{pmatrix} \omega_1^+ \\ \omega_2^+ \\ \omega_3^+ \end{pmatrix}, \quad (5c)$$

Here, $\alpha_{1,2,3}$ and $\delta_{1,2}$ are mixing angles that are taken real. To this end, we take stock of the independent parameters in the model. Having eliminated m_{11}^2, m_{22}^2 and m_{33}^2 through the tadpole conditions, there are the three dimensionful parameters m_{12}^2, m_{13}^2 and m_{23}^2 , the mix-

ing angles β, γ and twelve quartic couplings leading to a total of seventeen independent parameters in the gauge basis. However, the quartic couplings have been solved in terms of $\{\tan\beta, \tan\gamma, \delta_1, \delta_2, \alpha_1, \alpha_2, \alpha_3, m_{12}, m_{13}, m_{23}, M_h, M_{H_1}, M_{H_2}, M_{H_1^+}, M_{H_2^+}, M_{A_1}, M_{A_2}\}$ prompting us take the latter set as the independent parameters.

B. Yukawa sector

The possible Yukawa coupling schemes leading to flavour conservation in a 3HDM are listed in table IIB. Depending on the assignment of the charges, there can be five such types, namely (i) Type-I, (ii) Type-II, (iii) Type-X (lepton-specific), (iv) Type-Y (Flipped) and (v) Type-Z (democratic). It is seen that in Type-I 3HDM, up-type, down-type quarks and leptons only couple to scalar doublet ϕ_2 to acquire masses, whereas in Type-Z or democratic 3HDM, down-type, up-type quarks and leptons receive their masses through individual couplings with Φ_1, Φ_2 and Φ_3 respectively. For instance, an assignment of the $\mathbb{Z}_2 \times \mathbb{Z}'_2 \times \mathbb{Z}''_2$ charges responsible for a Type-Z 3HDM is

Scalar doublet	Type-I	Type-II	Lepton-specific	Flipped	Democratic
Φ_1	—	d, l	l	d	d
Φ_2	u, d, l	u	u, d	u, l	u
Φ_3	—	—	—	—	l

shown in table I.

Symmetry	Φ_1	Φ_2	Φ_3	Q_{L_i}, L_{L_i}	u_R	d_R	l_R
\mathbb{Z}_2	+	+	-	+	+	-	+
\mathbb{Z}'_2	+	-	+	+	-	+	+
\mathbb{Z}''_2	-	+	+	+	+	+	-

TABLE I: $\mathbb{Z}_2 \times \mathbb{Z}'_2 \times \mathbb{Z}''_2$ quantum numbers assigned to the doublets and fermions.

Next, we parameterise the interactions of the neutral scalar mass eigenstates with the fermions as follows.

$$\mathcal{L}_Y = \sum_{f=u,d,l} \left[-\frac{m_f}{v} \left\{ \sum_{\phi_S=h,H_1,H_2} y_f^{\phi_S} \bar{f} f \phi_S + \sum_{\phi_P=A_1,A_2} y_f^{\phi_P} \bar{f} i \gamma_5 f \phi_P \right\} \right] \quad (6)$$

Here, m_f refers to the mass of the fermion f , and, $y_f^{\phi_S}$ and $y_f^{\phi_P}$ are the Yukawa scale factors corresponding to the CP-even and CP-odd scalars respectively. These scale factors are expressible

in terms of the various mixing angles. We list the scale factors corresponding to h for all the 3HDM types in table II for illustration.

	Type-I	Type-II	Type-X	Type-Y	Type-Z
y_u^h	$\frac{s_{\alpha_1} c_{\alpha_2}}{s_{\beta} s_{\gamma}}$				
y_d^h	$\frac{s_{\alpha_1} c_{\alpha_2}}{s_{\beta} s_{\gamma}}$	$\frac{c_{\alpha_1} c_{\alpha_2}}{c_{\beta} s_{\gamma}}$	$\frac{s_{\alpha_1} c_{\alpha_2}}{s_{\beta} s_{\gamma}}$	$\frac{c_{\alpha_1} c_{\alpha_2}}{c_{\beta} s_{\gamma}}$	$\frac{c_{\alpha_1} c_{\alpha_2}}{c_{\beta} s_{\gamma}}$
y_l^h	$\frac{s_{\alpha_1} c_{\alpha_2}}{s_{\beta} s_{\gamma}}$	$\frac{c_{\alpha_1} c_{\alpha_2}}{c_{\beta} s_{\gamma}}$	$\frac{c_{\alpha_1} c_{\alpha_2}}{c_{\beta} s_{\gamma}}$	$\frac{s_{\alpha_1} c_{\alpha_2}}{s_{\beta} s_{\gamma}}$	$\frac{s_{\alpha_2}}{c_{\gamma}}$

TABLE II: Scale factors corresponding to the various Yukawa interactions involving h .

The interactions involving the charged eigenstates H_1^+ , H_2^+ and the quarks are quoted as

$$\mathcal{L}_{\text{charged}} = \sum_{i=1}^2 \left[\frac{\sqrt{2}V_{ud}}{v} \bar{u}(m_u A_u^i P_L - m_d A_d^i P_R) d H_i^+ + \text{h.c.} \right], \quad (7)$$

where V_{ud} and $P_L(P_R)$ respectively denote the CKM matrix element and the left (right) projection operator respectively. The expressions for A_u^i and A_d^i for the five 3HDM types taken are given in table III. We implement an exact alignment limit $\alpha_1 = \beta$, $\alpha_2 = \frac{\pi}{2} - \gamma$ in the ensuing sections in

	Type-I	Type-II	Type-X	Type-Y	Type-Z
A_u^1	$\frac{c_{\beta} c_{\delta_2} + c_{\gamma} s_{\beta} s_{\delta_2}}{s_{\beta} s_{\gamma}}$				
A_d^1	$\frac{c_{\beta} c_{\delta_2} + c_{\gamma} s_{\beta} s_{\delta_2}}{s_{\beta} s_{\gamma}}$	$\frac{-c_{\delta_2} s_{\beta} + c_{\beta} c_{\gamma} s_{\delta_2}}{s_{\gamma} c_{\beta}}$	$\frac{c_{\beta} c_{\delta_2} + c_{\gamma} s_{\beta} s_{\delta_2}}{s_{\beta} s_{\gamma}}$	$\frac{-c_{\delta_2} s_{\beta} + c_{\beta} c_{\gamma} s_{\delta_2}}{s_{\gamma} c_{\beta}}$	$\frac{-c_{\delta_2} s_{\beta} + c_{\beta} c_{\gamma} s_{\delta_2}}{s_{\gamma} c_{\beta}}$
A_u^2	$\frac{-c_{\delta_2} c_{\gamma} s_{\beta} + c_{\beta} s_{\delta_2}}{s_{\beta} s_{\gamma}}$				
A_d^2	$\frac{-c_{\delta_2} c_{\gamma} s_{\beta} + c_{\beta} s_{\delta_2}}{s_{\beta} s_{\gamma}}$	$\frac{-c_{\beta} c_{\delta_2} c_{\gamma} - s_{\beta} s_{\delta_2}}{s_{\gamma} c_{\beta}}$	$\frac{-c_{\delta_2} c_{\gamma} s_{\beta} + c_{\beta} s_{\delta_2}}{s_{\beta} s_{\gamma}}$	$\frac{-c_{\beta} c_{\delta_2} c_{\gamma} - s_{\beta} s_{\delta_2}}{s_{\gamma} c_{\beta}}$	$\frac{-c_{\beta} c_{\delta_2} c_{\gamma} - s_{\beta} s_{\delta_2}}{s_{\gamma} c_{\beta}}$

TABLE III: Expressions of A_u^i and A_d^i for five types of 3HDMs.

which case couplings of h to all SM particles become equal to the corresponding SM values.

III. THE $H_{1,2}^+$ W^-Z VERTEX AT ONE-LOOP

The amplitude for the decay $H_j^+ \rightarrow W^+ V$ ($j = 1, 2$) reads

$$\mathcal{M}_j = g M_W A_{jV}^{\mu\nu} \epsilon_{W\mu}^* \epsilon_{V\nu}^*, \quad (8)$$

where

$$A_{jV}^{\mu\nu} = g^{\mu\nu} F_{jV} + \frac{p_V^\mu p_W^\nu}{M_W^2} G_{jV} + i \epsilon^{\mu\nu\rho\sigma} \frac{p_{V\rho} p_{W\sigma}}{M_W^2} H_{jV}. \quad (9)$$

It is mentioned here that F_{jV}, G_{jV} and H_{jV} are the form-factors corresponding to the different Lorentz structures, and, p_W^ν, p_V^μ are the incoming momenta of W^\pm and V. To this end, we also introduce nonlinear gauge-fixing functions as [48–53]

$$\begin{aligned} f^+ &= (D_\mu^e + \frac{igs_W^2}{c_W} Z_\mu) W^{+\mu} - i\zeta M_W G^+, \\ f^Z &= \partial_\mu Z^\mu - \zeta M_Z G^0, \\ f^A &= \partial_\mu A^\mu. \end{aligned} \quad (10)$$

In the above, D_μ^e and ζ are the electromagnetic covariant derivative and gauge parameter respectively. It is noted that f^+ transforms covariantly under the electromagnetic gauge group and is nonlinear. The gauge-fixing Lagrangian involving f^+, f^Z and f^A can be written as:

$$\mathcal{L} = -\frac{1}{\zeta} f^+ f^- - \frac{1}{2\zeta} (f^Z)^2 - \frac{1}{2\zeta} (f^A)^2. \quad (11)$$

One observes that setting $\zeta = 1$ removes the unphysical $G^+ W^- Z(\gamma)$ vertices from the framework. The same also entails that the Feynman rules for the $Z(\gamma) W^+ W^-$ trilinear gauge vertices gets modified to

$$\Gamma_{\rho\nu\mu}^{\gamma W^+ W^-}(k, p, q) = -ie[g_{\mu\nu}(k - p - q)_\rho + g_{\nu\rho}(p - q)_\mu + g_{\rho\mu}(q - k + p)_\nu], \quad (12a)$$

$$\Gamma_{\rho\nu\mu}^{ZW^+ W^-}(k, p, q) = -igc_W[g_{\mu\nu}(k - p + \frac{s_W^2}{c_W^2}q)_\rho + g_{\nu\rho}(p - q)_\mu + g_{\rho\mu}(q - k - \frac{s_W^2}{c_W^2}p)_\nu]. \quad (12b)$$

We are now in a position to discuss the contribution of a 3HDM to the form factors F_{jZ}, G_{jZ} and H_{jZ} for $j = 1, 2$. A generic $H_j^+ W^- Z$ one-loop amplitude contains one power of a trilinear coupling at one vertex and two powers of gauge couplings from the remaining vertex (vertices), as is shown in the past studies [10–14]. This allows for arranging all the one-loop diagrams into UV-finite and gauge-invariant subsets. We display below, for instance, all diagrams featuring the $H_1 - H_1^+ - H_1^-$ trilinear interaction (denoted by $\lambda_{H_1 H_1^+ H_1^-}$) in an exact alignment. We elucidate on the topology of each diagram. Diagrams E_1 and E'_1 are bubble topologies containing a 4-point $S_i S_j W^+ Z$ vertex and a 3-point $W^+ W^- Z$ vertex respectively, where S_i is a generic scalar. On the other hand, L_1, M_1 and N_1 are triangle topologies involving two $S_i S_j V$ vertices. The amplitudes corresponding to the aforesaid five diagrams are calculated in $d = 4 - \epsilon$ dimensions with μ being the dimensional regularisation scale, and, expressed in terms of Passarino-Veltman functions [54]

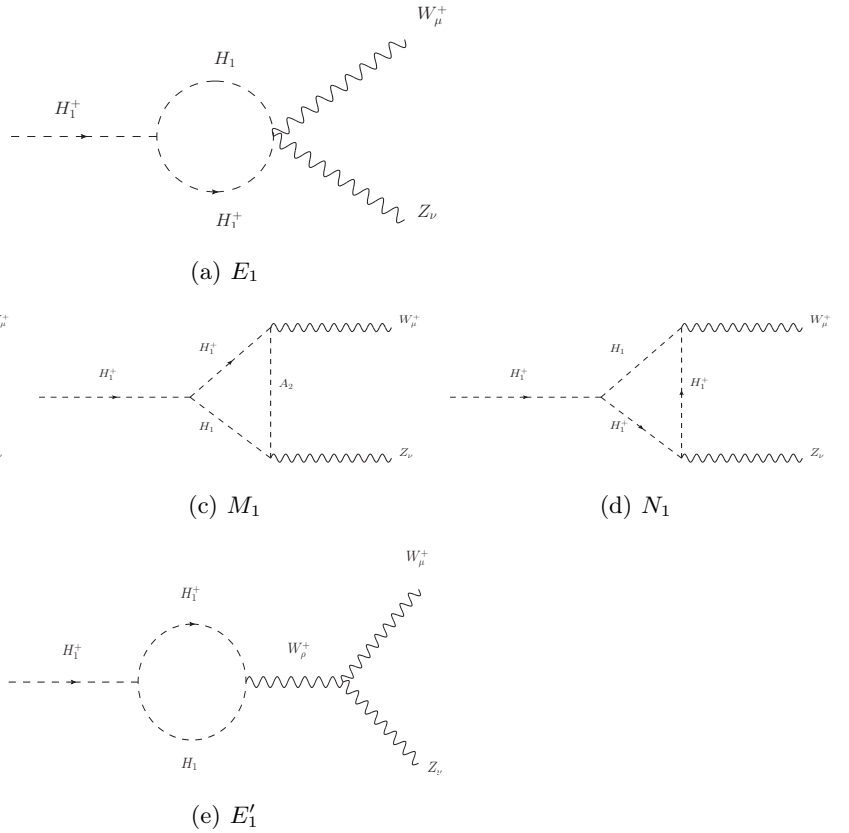


FIG. 1:

below. We also indicate the corresponding UV-divergent parts.

$$\begin{aligned} (F_{1Z})_{E_1} &= \frac{1}{16\pi^2 v} \frac{s_W^2}{c_W} c_{\alpha_3+\delta_2} \lambda_{H_1^+ H_1^- H_1} B_0(H_1^+; H_1^+, H_1) \\ &\xrightarrow{\text{UV-divergent}} \frac{1}{16\pi^2 v} \frac{s_W^2}{c_W} c_{\alpha_3+\delta_2} \lambda_{H_1^+ H_1^- H_1} (\text{div}) \end{aligned} \quad (13a)$$

$$\begin{aligned} (F_{1Z})_{L_1} &= \left(\frac{-2\lambda_{H_1^+ H_1^- H_1}}{16\pi^2 v c_W} \right) (c_{\delta_1-\delta_2} c_{\alpha_3+\delta_1}) C_{24}(W, Z, H_1^+; H_1^+, A_1, H_1) \\ &\xrightarrow{\text{UV-divergent}} \left(\frac{-2\lambda_{H_1^+ H_1^- H_1}}{16\pi^2 v c_W} \right) (c_{\delta_1-\delta_2} c_{\alpha_3+\delta_1}) \left(\frac{\text{div}}{4} \right) \end{aligned} \quad (13b)$$

$$\begin{aligned} (F_{1Z})_{M_1} &= \left(\frac{-2\lambda_{H_1^+ H_1^- H_1}}{16\pi^2 v c_W} \right) (s_{\delta_1-\delta_2} s_{\alpha_3+\delta_1}) C_{24}(W, Z, H_1^+; H_1^+, A_2, H_1) \\ &\xrightarrow{\text{UV-divergent}} \left(\frac{-2\lambda_{H_1^+ H_1^- H_1}}{16\pi^2 v c_W} \right) (s_{\delta_1-\delta_2} s_{\alpha_3+\delta_1}) \left(\frac{\text{div}}{4} \right) \end{aligned} \quad (13c)$$

$$\begin{aligned} (F_{1Z})_{N_1} &= \left(\frac{2c_{2W}}{c_W} \right) \frac{\lambda_{H_1^+ H_1^- H_1}}{16\pi^2 v} (c_{\alpha_3+\delta_2}) C_{24}(W, Z, H_1^+; H_1, H_1^+, H_1^+) \\ &\xrightarrow{\text{UV-divergent}} \left(\frac{2c_{2W}}{c_W} \right) \frac{\lambda_{H_1^+ H_1^- H_1}}{16\pi^2 v} (c_{\alpha_3+\delta_2}) \left(\frac{\text{div}}{4} \right), \end{aligned} \quad (13d)$$

$$\begin{aligned} (F_{1Z})_{E'_1} &= \frac{1}{16\pi^2 v} \frac{s_W^2}{c_W} c_{\alpha_3+\delta_2} \lambda_{H_1^+ H_1^- H_1} [B_0(H_1^+; H_1^+, H_1) + 2B_1(H_1^+; H_1^+, H_1)] \\ &\xrightarrow{\text{UV-divergent}} 0. \end{aligned} \quad (13e)$$

A quantity P appearing in the arguments of the Passarino-Veltman functions in Eqs.(13) refers to the squared mass M_P^2 . We refer to the Appendix for expressions of the various Passarino-Veltman functions and dub $\frac{2}{\epsilon} - 4\pi + \gamma_E + \ln(\mu^2)$ as the quantity "div". It can be straightforwardly checked that UV-divergent and μ -dependent parts of $(F_{1Z})_{E_1} + (F_{1Z})_{L_1} + (F_{1Z})_{M_1} + (F_{1Z})_{N_1} + (F_{1Z})_{E'_1}$ vanishes

In addition to checking for UV-finiteness, gauge invariance of an $H_j^+ W^- \gamma$ vertex can serve as a useful check of the $H_j^+ W^- Z$ amplitude even if a detailed quantification of the former in a given model is not explicitly aimed at. The Ward identity enforces $A_{j\gamma}^{\mu\nu} p_{\gamma\nu} = 0$ that ultimately leads to

$$F_{j\gamma} = \frac{G_{j\gamma}}{2} \left(1 - \frac{M_{H_j^+}^2}{M_W^2} \right). \quad (14)$$

The amplitudes featuring a given trilinear coupling would form a UV-finite subset in case of $H_j^+ \rightarrow W^+ \gamma$ too. The diagrams corresponding to the $H_1 - H_1^+ - H_1^-$ trilinear coupling are named R_1 , S_1 and R'_1 and are displayed below. We define the dimensionless quantity $\Omega_j = \frac{2F_{j\gamma}}{G_{j\gamma}} \left(1 - \frac{M_{H_j^+}^2}{M_W^2} \right)^{-1}$

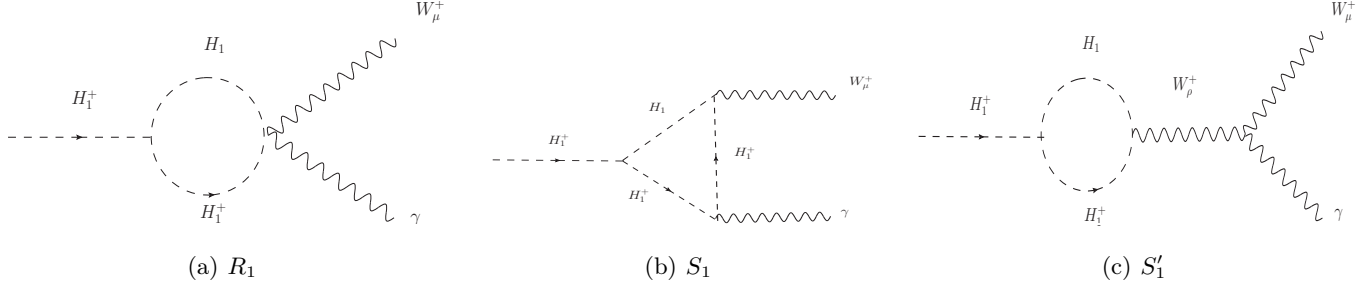


FIG. 2:

with a numerical cross-check in view. The aforementioned set of amplitudes then gives

$$\Omega_1 = - \left\{ \frac{B_0(H_1^+; H_1^+, H_1) - 2C_{24}(H_1^+, W, 0; H_1, H_1^+, H_1^+) + B_1(H_1^+; H_1^+, H_1)}{C_{12}(H_1^+, W, 0; H_1, H_1^+, H_1^+) + C_{23}(H_1^+, W, 0; H_1, H_1^+, H_1^+)} \right\} \left(1 - \frac{M_{H_1^+}^2}{M_W^2} \right)^{-1} \quad (15)$$

We numerically evaluate Ω_1 using the publicly available tool `LoopTools` [55] with $M_{H_1^+} = 200$ GeV and M_{H_1} varied in the [200 GeV, 1 TeV] range. Treating $|\Omega_1 - 1|$ as a measure of breakdown of gauge invariance, we display the behaviour of the same *w.r.t.* M_{H_1} in Fig. 3. The deviation turns

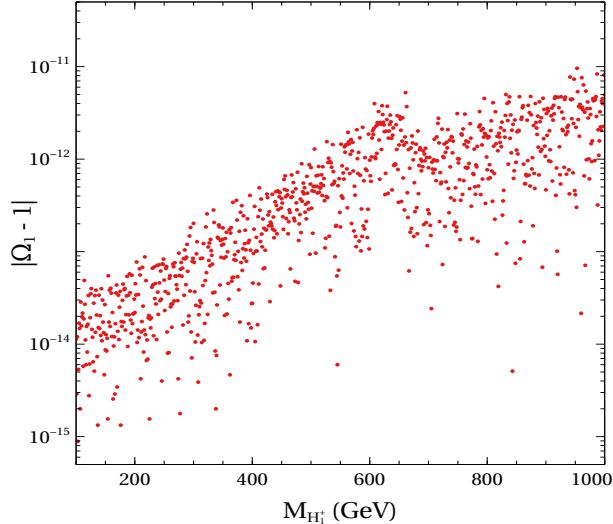


FIG. 3:

out to be tiny and is mostly an artefact of numerical accuracy. Thus, it is safely concluded that the $H_j^+ W^- \gamma$ amplitude stemming from R_1, S_1 and S'_1 is consistent with Ward identity. We argue here that such an observation for R_1, S_1 and S'_1 also serves as an additional check on the correctness of E_1, L_1, M_1, N_1, E'_1 , given the similarities of the two sets of amplitudes at one-loop.

In all, it is demonstrated that $H_j^+ \rightarrow W^+ Z$ amplitudes featuring a given scalar trilinear interaction constitute a UV-finite and gauge invariant subset. Therefore, in view of the large number

of amplitudes in this framework, we cluster them according to the trilinear couplings in Tables IV (H₁⁺ decay) and V (H₂⁺ decay).

Trilinear interaction	Diagrams
H ₁ – H ₁ ⁺ – H ₁ ⁻	E ₁ , L ₁ , M ₁ , N ₁ , E' ₁
H ₁ – H ₁ ⁺ – H ₂ ⁻	E ₂ , L ₂ , M ₂ , N ₂ , E' ₂
H ₂ – H ₁ ⁺ – H ₁ ⁻	E ₃ , L ₃ , M ₃ , N ₃ , E' ₃
H ₂ – H ₁ ⁺ – H ₂ ⁻	E ₄ , L ₄ , M ₄ , N ₄ , E' ₄
A ₁ – H ₁ ⁺ – H ₂ ⁻	O ₁ , X ₁ , Y ₁ , Z ₁ , O' ₁
A ₂ – H ₁ ⁺ – H ₂ ⁻	O ₂ , X ₂ , Y ₂ , Z ₂ , O' ₂

TABLE IV: Serial numbers of scalar 1-loop amplitudes for H₁⁺ → W⁺Z

Trilinear interaction	Diagrams
H ₁ – H ₁ ⁺ – H ₁ ⁻	E ₅ , L ₅ , M ₅ , N ₅ , E' ₅
H ₁ – H ₁ ⁺ – H ₂ ⁻	E ₆ , L ₆ , M ₆ , N ₆ , E' ₆
H ₂ – H ₁ ⁺ – H ₁ ⁻	E ₇ , L ₇ , M ₇ , N ₇ , E' ₇
H ₂ – H ₁ ⁺ – H ₂ ⁻	E ₈ , L ₈ , M ₈ , N ₈ , E' ₈
A ₁ – H ₁ ⁺ – H ₂ ⁻	O ₃ , X ₃ , Y ₃ , Z ₃ , O' ₃
A ₂ – H ₁ ⁺ – H ₂ ⁻	O ₄ , X ₄ , Y ₄ , Z ₄ , O' ₄

TABLE V: Serial numbers of scalar 1-loop diagrams for H₂⁺ → W⁺Z

Fermionic contributions at one-loop to H_j⁺ → W⁺Z are shown in the Appendix. Next, the decay width for H_j⁺ → W⁺Z reads

$$\Gamma(H_j^+ \rightarrow W^+Z) = M_{H_j^+} \frac{\sqrt{\lambda(1, \omega_j, z_j)}}{16\pi} \sum_{i=L,T} |M_{ii}|_j^2, \quad (16)$$

Here $\lambda(a, b, c) = (a - b - c)^2 - 4abc$, $\omega_j = \frac{M_W^2}{M_{H_j^+}^2}$, $z = \frac{M_Z^2}{M_{H_j^+}^2}$. In addition, L and T refer to the longitudinal and transverse polarizations respectively. The longitudinal and transverse squared amplitudes are given by

$$\begin{aligned} |M_{LL}|_j^2 &= \frac{g^2}{4z_j} |(1 - \omega_j - z_j)F_{jZ} + \frac{\lambda(1, \omega_j, z_j)}{2\omega_j} G_{jZ}|^2, \\ |M_{TT}|_j^2 &= g^2 (2\omega_j |F_{jZ}|^2 + \frac{\lambda(1, \omega_j, z_j)}{2\omega_j} |H_{jZ}|^2). \end{aligned} \quad (17)$$

IV. CONSTRAINTS

We parameter space of a flavour-conserving 3HDM is subjected to the following theoretical and experimental constraints.

A. Theoretical Constraints

A perturbative framework stipulates that the magnitude of the quartic couplings remains bounded from above at 4π , that is $|\lambda_i| \leq 4\pi$. The corresponding bound on a Yukawa coupling is $|y| \leq \sqrt{4\pi}$. Next, the scalar potential remains bounded from below along various directions in field space if the following conditions are satisfied.

$$\begin{aligned} \lambda_1 > 0, \quad \lambda_2 > 0, \quad \lambda_3 > 0, \quad \lambda_{12} + \sqrt{\lambda_1 \lambda_2} > 0, \quad \lambda_{23} + \sqrt{\lambda_2 \lambda_3} > 0, \quad \lambda_{13} + \sqrt{\lambda_1 \lambda_3} > 0, \\ \lambda_{12} + \lambda'_{12} - |\lambda''_{12}| + \sqrt{\lambda_1 \lambda_2} > 0, \quad \lambda_{23} + \lambda'_{23} - |\lambda''_{23}| + \sqrt{\lambda_2 \lambda_3} > 0, \quad \lambda_{13} + \lambda'_{13} - |\lambda''_{13}| + \sqrt{\lambda_1 \lambda_3} > 0 \end{aligned} \quad (18)$$

The theoretical constraint taken up next is perturbative unitarity. Various $2 \rightarrow 2$ scattering amplitudes involving longitudinal components of gauge bosons can be mapped to ones involving the Goldstone bosons using the electroweak equivalence theorem [56, 57]. The latter amplitudes, expressible in terms of the scalar quartic couplings, can be arranged in the form of a matrix. The framework obeys perturbative unitarity if the eigenvalues of the aforementioned matrix have magnitudes not exceeding 8π . For a 3HDM, one can construct the amplitudes using neutral and singly-charged two-particle states, which themselves comprise of the scalar fields ω_i^\pm, h_i, z_i (with $i = 1, 2, 3$) in the gauge basis. This in turn leads to 30×30 and 18×18 scattering matrices in the bases of two-particle neutral and singly charged bases respectively [58].

It is cumbersome to extract the eigenvalues analytically. Therefore, we adopt another approach for a 3HDM. The details are relegated in the Appendix. This new approach furnishes analytical forms for the following 18 eigenvalues.

$$\begin{aligned} \lambda_{12} \pm \lambda'_{12}, \quad \lambda_{12} \pm \lambda''_{12}, \quad \lambda_{13} \pm \lambda'_{13}, \quad \lambda_{13} \pm \lambda''_{13}, \quad \lambda_{23} \pm \lambda'_{23}, \quad \lambda_{23} \pm \lambda''_{23}, \\ \lambda_{12} + 2\lambda'_{12} \pm 3\lambda''_{12}, \quad \lambda_{13} + 2\lambda'_{13} \pm 3\lambda''_{13}, \quad \lambda_{23} + 2\lambda'_{23} \pm 3\lambda''_{23} \end{aligned} \quad (19)$$

Nine more eigenvalues are obtained from three 3×3 matrices as detailed in the Appendix.

B. Experimental Constraints

1. $h \rightarrow \gamma\gamma$ signal strength

The $h \rightarrow \gamma\gamma$ decay width can deviate from the corresponding SM value in spite of an exact alignment on account of the additional one-loop contributions coming from $H_{1,2}^+$. The corresponding amplitude and decay width read [59, 60]:

$$\begin{aligned}\mathcal{M}_{h \rightarrow \gamma\gamma}^{\text{3HDM}} &= \sum_f N_f Q_f^2 y_f^h A_{1/2}\left(\frac{M_h^2}{4M_f^2}\right) + f_{VV}^h A_1\left(\frac{M_h^2}{4M_W^2}\right) \\ &\quad + \sum_{i=j}^2 \frac{\lambda_{hH_i^+H_i^-} v}{2M_{H_j^+}^2} A_0\left(\frac{M_h^2}{4M_{H_i^+}^2}\right)\end{aligned}\tag{20a}$$

$$\Gamma_{h \rightarrow \gamma\gamma}^{\text{3HDM}} = \frac{G_F \alpha^2 M_h^3}{128\sqrt{2}\pi^3} |\mathcal{M}_{h \rightarrow \gamma\gamma}^{\text{3HDM}}|^2,\tag{20b}$$

where N_f and Q_f respectively denote respectively color factor, charge of fermion f . Additionally, G_F and α are the Fermi-constant and the QED fine-structure constant respectively. Moreover, $f_{VV}^h = c_\gamma s_{\alpha_2} + c_{\alpha_2} c_{\alpha_1 - \beta} s_\gamma$ is the scale factor corresponding to the $h - V - V$ coupling. One however notes $y_f^h = f_{VV}^h = 1$ for alignment. The functions $A_0(x)$, $A_{1/2}(x)$ and $A_1(x)$ are given in [59, 60]. Given the production cross section of h is unchanged *w.r.t.* the SM for an exact alignment, the signal strength for the $h \rightarrow \gamma\gamma$ channel becomes

$$\mu_{\gamma\gamma} \simeq \frac{\Gamma_{\text{3HDM}}(h \rightarrow \gamma\gamma)}{\Gamma_{\text{exp}}(h \rightarrow \gamma\gamma)}.\tag{21}$$

We have implemented this constraint at the 2σ -level following the latest measurements from CMS [61] and ATLAS [62].

2. Electroweak Precision Observables

A multi-Higgs setup induces additional contributions to the oblique (S, T, U) parameters [63–65].

The latest limits on ΔS and ΔT for $\Delta U = 0$ are

$$\Delta S = 0.05 \pm 0.08, \quad \Delta T = 0.09 \pm 0.07, \quad \rho_{ST} = 0.92.\tag{22}$$

We have calculated the corresponding contributions coming from a $\mathbb{Z}_2 \times \mathbb{Z}'_2 \times \mathbb{Z}''_2$ 3HDM following [66] and imposed the aforementioned limit at 2σ .

3. $B \rightarrow X_s\gamma$ decay

The most stringent flavour constraint for a multi-doublet framework that forbids tree level FCNCs arises from the $B \rightarrow X_s\gamma$ branching ratio. SM predicts the aforesaid ratio to be $(3.36 \pm 0.23) \times 10^{-4}$ while its experimental average is $(3.32 \pm 0.16) \times 10^{-4}$. NP contributions to the $b \rightarrow s\gamma$ amplitude thus get tightly constrained. Such contributions stem from $H_{1,2}^+$ in a 3HDM and modify the $C_{7,8}$ Wilson coefficients *w.r.t.* the SM values. Following [67], one has the following at a matching scale $\simeq 160$ GeV

$$\delta C_{7,8}^{\text{eff}} = \sum_{j=1,2} \left[\frac{(A_u^j)^2}{3} F_{7,8}^{(1,2)}(x_j) - A_u^j A_d^j F_{7,8}^{(1,2)}(x_j) \right]. \quad (23)$$

One notes that $x_j = M_t^2/M_{H_j^+}^2$ and

$$F_7^{(1)}(x) = \frac{x(7-5x-8x^2)}{24(x-1)^3} + \frac{x^2(3x-2)}{4(x-1)^4} \ln x, \quad (24a)$$

$$F_8^{(1)}(x) = \frac{x(2+5x-x^2)}{8(x-1)^3} - \frac{3x^2}{4(x-1)^4} \ln x. \quad (24b)$$

$$F_7^{(2)}(x) = \frac{x(3-5x)}{12(x-1)^2} + \frac{x(3x-2)}{6(x-1)^3} \ln x, \quad (24c)$$

$$F_8^{(2)}(x) = \frac{x(3-x)}{4(x-1)^2} - \frac{x}{2(x-1)^3} \ln x. \quad (24d)$$

The factors A_u^j and A_d^j are expressed in Table III for the 3HDM types considered. Following [36,38 of Avik], the limits on the branching ratio translate into

$$-0.063 \leq \delta C_7^{\text{eff}} + 0.24 \delta C_8^{\text{eff}} \leq 0.073. \quad (25)$$

V. NUMERICAL SCANS AND EVALUATION OF THE FORM FACTORS

This section is devoted to sampling the 3HDM parameter space *w.r.t.* the said constraints and evaluating the $H_{1,2}^+ \rightarrow W^+Z$ form factors numerically. And we choose the Type-II, lepton specific and democratic 3HDM in view of the difference in the Yukawa structures. Drawing analogies with the 2HDM, a few comments are in order. First, the stringent $M_{H^+} \geq 580$ GeV limit from $B \rightarrow X_s\gamma$ for a Type-II 2HDM is expected to appropriately relax in the 3HDM, thanks to cancellations in the amplitude level. It is worthwhile to examine the form factors for the comparatively lighter H_1^+ or H_2^+ in foresight. Secondly, the $B \rightarrow X_s\gamma$ branching fraction is identical in the Type-I and lepton specific 3HDM owing to the identical quark couplings in the two cases. We choose the latter in view of its potentially enhanced lepton Yukawas. We also keep in mind a possible scope to search for

$H_{1,2}^+$ at colliders through their lepton couplings. Finally, the democratic 3HDM has also generated interest [DD, Moretti etc] on account of its enticing Yukawa structure where the u-quark, b-quark and lepton masses come from three different scalar doublets.

Before embarking on the numerical scans, it is pointed out that an elaborate sweep of the 3HDM parameter space becomes computationally hectic given the large number of free parameters. Some past studies [Coleppa etc] have carried out detailed investigations in this direction. We therefore follow a more economical approach in this paper. First, we implement an exact alignment limit as $\alpha_1 = \beta$, $\alpha_2 = \frac{\pi}{2} - \gamma$. Secondly, we fix $M_{H_1} = M_{H_1^+}$, $M_{H_2} = M_{H_2^+}$, $\delta_1 = \delta_2$, $\alpha_3 = -\delta_2$. in order to ensure $\Delta T = 0$. The rest of the parameters are varied as under:

$$\begin{aligned} 0 &\leq m_{12}, m_{23}, m_{13} \leq 500 \text{ GeV}, \\ 100 \text{ GeV} &\leq M_{H_1^+}, M_{H_2^+}, M_{A_1}, M_{A_2} \leq 1000 \text{ GeV}, \\ 1 &\leq \tan \gamma, \tan \beta \leq 20, \quad 0 \leq \delta_2 \leq 2\pi. \end{aligned} \tag{26}$$

We adopt the following sequence in accepting parameter points. (i) The first set of points ensure perturbative unitarity and ensure a bounded-from-below potential. (ii) From the first set, we screen the points that satisfy the $h \rightarrow \gamma\gamma$ constraint, and finally, (iii) we further select those points that successfully negotiate the bound on the $B \rightarrow X_s\gamma$ branching ratio. The parameter points allowed at each of the aforesaid stages are plotted for the Type-II and lepton-specific 3HDMs in Fig.4 and Fig.5.

An inspection reveals that the allowed parameter spaces for the two 3HDMs mainly differ in terms of the allowed values of the charged Higgs masses. While the $B \rightarrow X_s\gamma$ constraint does not constrain $M_{H_1^+}$ and $M_{H_2^+}$ for the lepton-specific case, it rules out simultaneously low masses for the two charged Higgses.

Fig.6-8 depict 2D color-coded scatter plots in $|F_{1Z}| - |F_{2Z}|$ plane with the colour bar indicating the scalar mass splitting $|M_{A_2} - M_{H_2^+}|$. As can be seen from the plots, the mass splitting $|M_{A_2} - M_{H_2^+}|$ plays a crucial role in determining the strength of one-loop contributions to $H_{1,2}^+ W^- Z$ vertices. The strong sensitivity to the scalar mass splittings is expected due to the custodial symmetry breaking effects. If the splitting is large, the custodial symmetry breaking effects get amplified, producing larger loop contributions. Therefore for the larger mass splittings, $|F_{1(2)Z}|$ are large for all three types of 3HDMs, thereby the yellow points populate the upper parts of the $|F_{1Z}| - |F_{2Z}|$ plane in Fig.6-8.

The scatter plots in $|F_{1Z}| - |F_{2Z}|$ plane exhibit a strong positive correlation for all benchmark choices in all three types of 3HDMs. In particular, the parameter points with larger values of $|F_{1Z}|$

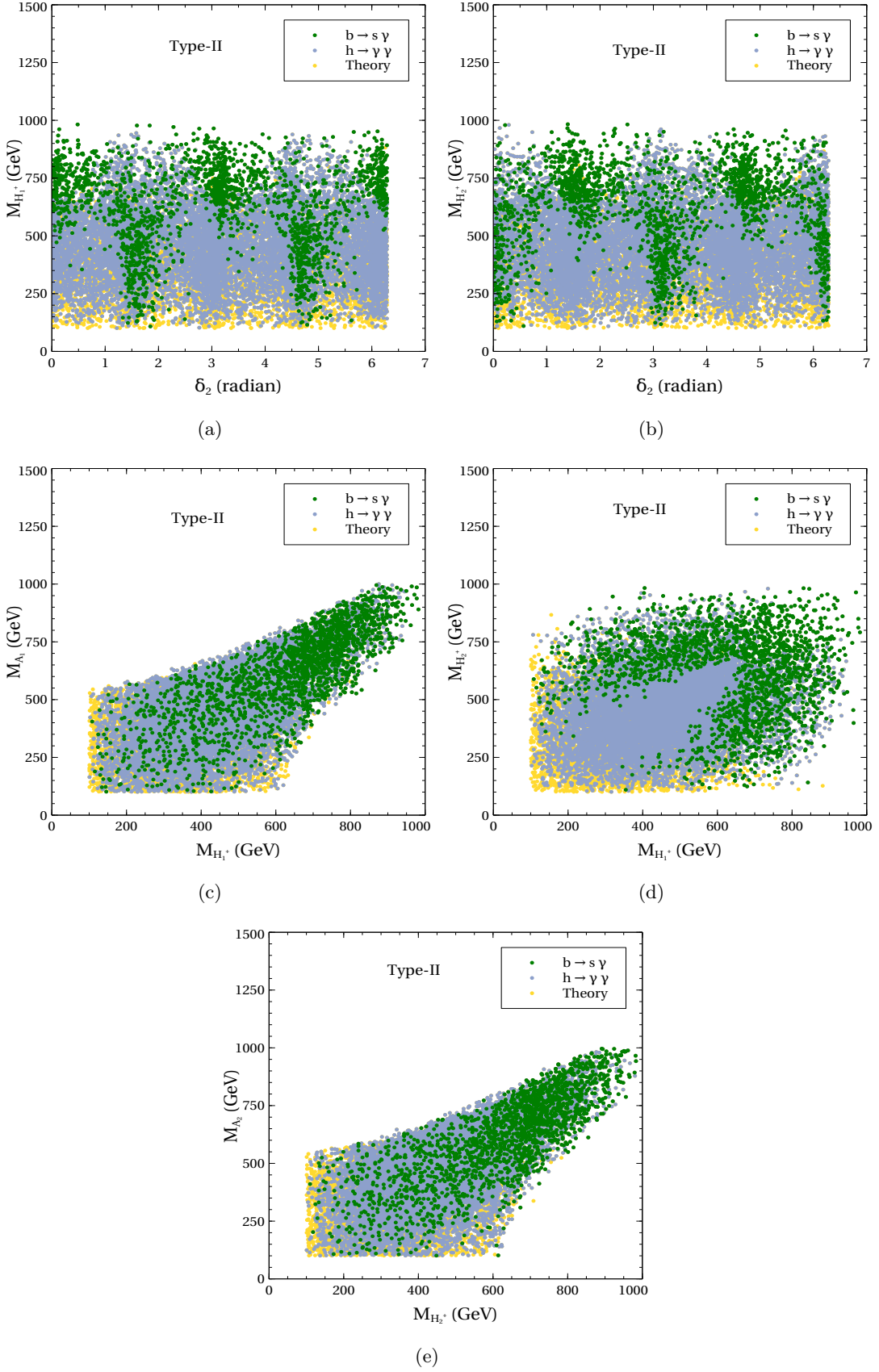


FIG. 4: Allowed parameter points for the Type-II 3HDM. The color-coding is explained in the legends.

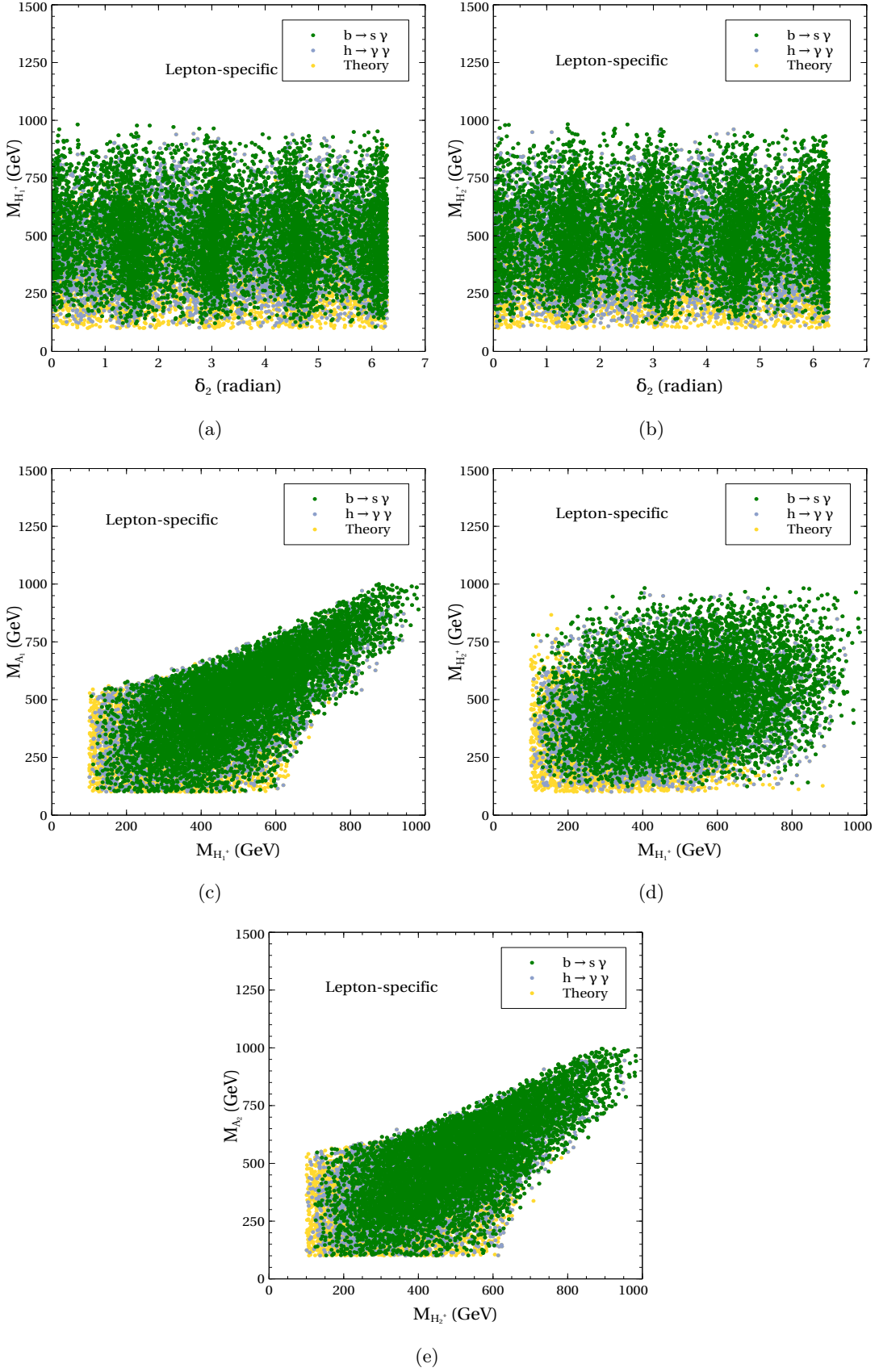


FIG. 5: Allowed parameter points for the lepton-specific 3HDM. The color-coding is explained in the legends.

systematically correspond to larger values of $|F_{2Z}|$. The logic behind this correlation is that, both the contributions to $|F_{1Z}|$ and $|F_{2Z}|$ originate from the same diagrams involving same particles. Thus the mass splittings affect both the form factors in a correlated manner, not independently.

With the increase in charged Higgs masses, the strength of form factor decreases and this feature remains same for all variants of 3HDMs. Thus larger values of $M_{H_1^+}$ and $M_{H_2^+}$, the allowed regions in the $|F_{1Z}| - |F_{2Z}|$ planes gradually shrink toward the origin. For lighter charged Higgs masses, due to smaller loop suppression, the form factors attain higher values. Thus for the scenarios with $M_{H_{1(2)}^+} \sim 175 - 200$ GeV, the allowed points cluster towards the upper edges of the scatter plots, where as increase of the masses to 300 GeV or beyond leads to a noticeable reduction in the attainable magnitudes of form factors.

The basic nature of the 2D colour-coded scatter plots in $|G_{1Z}| - |G_{2Z}|$ plane for the same set of charged Higgs masses and mass splitting $|M_{A_2} - M_{H_2^+}|$ mimics that of the plots in $|F_{1Z}| - |F_{2Z}|$ plane, apart from the magnitude. The magnitude of $G_{1(2)Z}$ is approximately one order of magnitude less than the magnitude of $F_{1(2)Z}$ due to the momentum-suppressed nature of the Lorentz structures.

It is evident from the numerical analysis that the magnitudes of the form factors $|F_{1Z}|$ and $|F_{2Z}|$ strongly depend on the charged Higgs masses $M_{H_1^+}$ and $M_{H_2^+}$ and mildly sensitive on the variants of 3HDMs. For $M_{H_2^+} \sim 175 - 200$ GeV and $M_{H_2^+} \sim 400 - 500$ GeV, $|F_{1Z}|$ and $|F_{2Z}|$ span the range: $|F_{1Z}|, |F_{2Z}| \sim 1 \times 10^{-2} - 5 \times 10^{-2}$, with the upper end of this range corresponding to scenarios with sizable charged-neutral scalar mass splittings. With the increase of $M_{H_2^+} \sim 300$ GeV, the magnitudes decreases as: $|F_{1Z}|, |F_{2Z}| \sim 2 \times 10^{-2}$. For heavy scalars, *i.e.* $M_{H_1^+} \geq 650$ GeV and $M_{H_2^+} \geq 500$ GeV, the magnitudes of $|F_{1Z}|, |F_{2Z}|$ further decrease below 10^{-2} . For $M_{H_1^+} = M_{H_2^+}$, the plots show a symmetric nature of the allowed parameter space in the $|F_{1Z}| - |F_{2Z}|$ plane. This symmetry arises because the loop amplitudes depend only on mass differences and mixing combinations, which become invariant under the interchange of the two charged Higgs states in the degenerate limit. Consequently, no charged scalar is kinematically or dynamically preferred, leading to symmetric parameter distributions.

Although the scalar mass spectrum primarily controls the strength of the one-loop contributions, there is a subdominant but non-negligible effect coming from different variants of 3HDMs. This is by the virtue of different Yukawa couplings between the charged Higgses and fermions, which enter into the diagrams and contribute to the fermionic counter part of one-loop form factors. Since in type-II and democratic 3HDM, Φ_1 and Φ_2 couple with down-type and up-type quarks respectively and the coupling with lepton is different, the strength of the fermionic counterpart contributing to the form factors appears to be almost same. That is why, the plots in Fig.6 and Fig.8 depict

the same nature and magnitude of the form factors for a given value of charged Higgs masses and charged-neutral scalar mass splitting. On the contrary, for lepton-specific 3HDM, where both up-type and down-type quarks couple with Φ_2 , there is slight suppression in the maximal attainable values of the form factors compared to the other two aforementioned variants.

VI. OBSERVABILITY AT THE LHC

This section discusses possible signals at the LHC that can be potential probes of the $H_{1,2}^+ W^- Z$ vertex. It is mentioned at the outset that the $gb \rightarrow tH^+$ process can have a sizeable production cross section in 2HDMs. And a subsequent $H^+ \rightarrow W^+ Z$ decay can shed light on the $H^+ W^- Z$ coupling. This has been studied before in 2HDMs [Gauhar, Kanemura] and its extensions [15, 46]. It is reported that $\sigma_{gb} \times \text{BR}_{H^+ \rightarrow W^+ Z}$ can be $\mathcal{O}(0.1)$ fb for $M_{H^+} < M_t + M_b$ and as large as $\mathcal{O}(100)$ fb) for $M_{H^+} > M_t + M_b$.

Signatures of 3HDMs have been studied at the colliders, a partial list of which is [68–77]. In this study, we focus on $H_{1,2}^+$ production using WZ fusion as shown below in Fig.9. The motivation is to probe the radiative $H_{1,2}^+ W^- Z$ vertices at the production level itself. The fact that we have numerical estimates of the one-loop form factors for both H_1^+ and H_2^+ at this point gives us the scope to compare the corresponding WZ production rates. We implement the model in **FeynRules** [78, 79] and extract an Universal FeynRules Output [80]. The same is passed on to **MadGraph5 aMC@NLO** [81] and $pp \rightarrow H_{1,2}^\pm jj$ is subsequently generated. It is added that the **NN23L01** parton distribution function (PDF) is used to compute the cross sections at the 14 TeV LHC². Moreover, the cuts $p_T^j > 20$ GeV, $|\eta_j| < 5$ and $\Delta R_{jj} > 0.4$ are applied at the time of generation. We look for the subsequent decays $H_{1,2}^+ \rightarrow t\bar{b}$, $\tau\bar{\nu}$, $W^+ Z$. The $\sigma \times \text{BR}$ values are accordingly estimated for the lepton specific 3HDM for specific values of the charged Higgs masses. We choose $(M_{H_1^+}, M_{H_2^+}) = (175 \text{ GeV}, 175 \text{ GeV}), (200 \text{ GeV}, 200 \text{ GeV}), (500 \text{ GeV}, 500 \text{ GeV})$ for illustration. The values of $\sigma \times \text{BR}$ are shown in a scatter plot for the allowed parameter points in Fig.10. The $H_{1,2}^+ \rightarrow t\bar{b}$ decay is kinematically blocked for $H_{1,2}^+$ having mass 175 GeV. The $pp \rightarrow H_{1,2}^\pm \rightarrow \tau\nu$ cross section dominates over $pp \rightarrow H_{1,2}^\pm \rightarrow W^\pm Z$ for most of the parameter space and the former cross section can reach up to $\mathcal{O}(0.1)$ fb). Despite the $t\bar{b}$ mode opening up for $M_{H_1^+} = M_{H_2^+} = 200$ GeV, it is seen that the $\tau\nu$ mode can still dominate. And this higher leptonic branching fraction is traced back to the enhanced leptonic Yukawas in the lepton-specific case. However, the $t\bar{b}$ mode takes over for higher charged

² An LO PDF such as NN23LO1 must be used for computing LO cross sections like what we have done here.

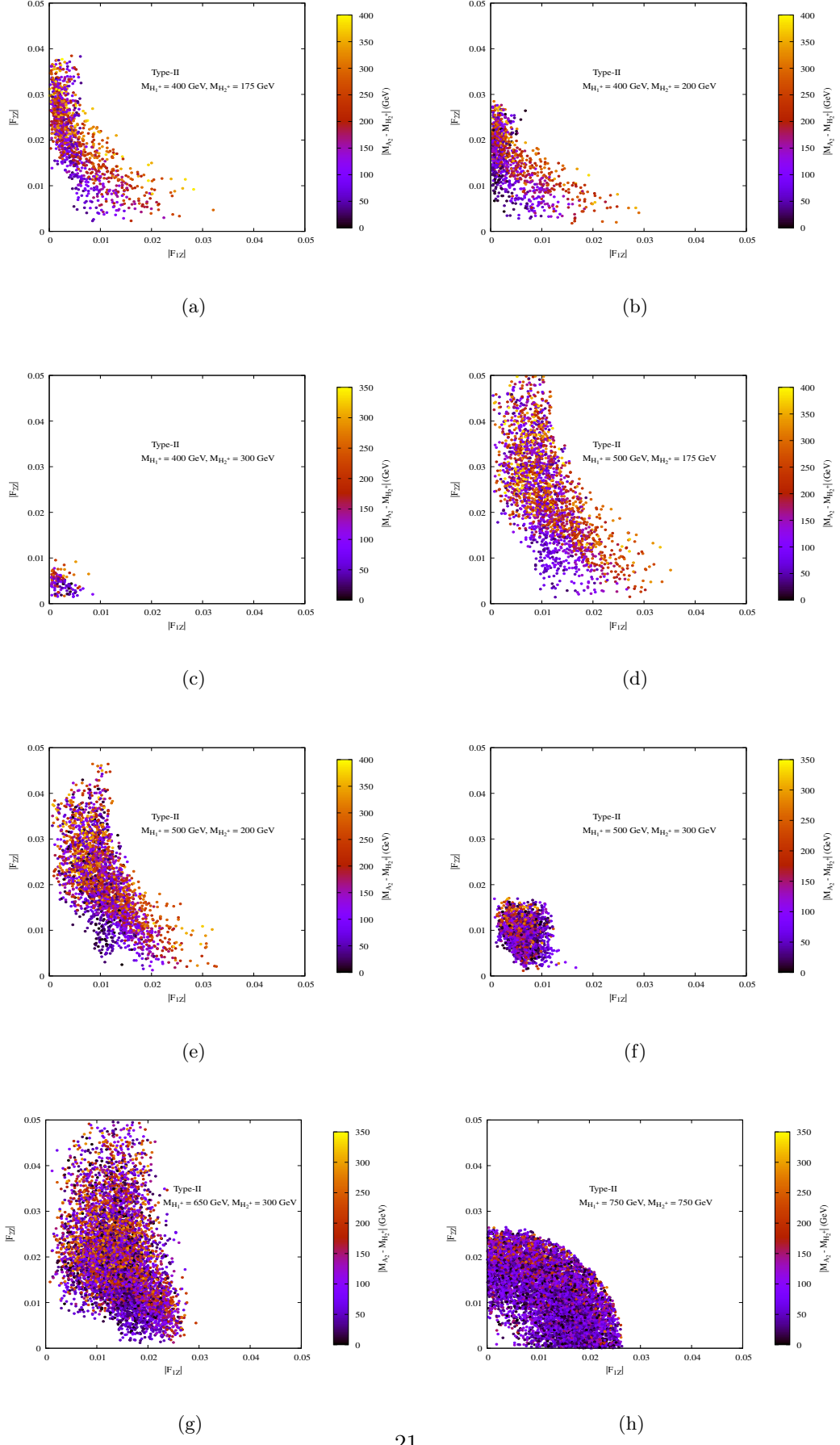


FIG. 6: $|F_{2Z}|$ vs. $|F_{1Z}|$ plots for different values of $M_{H_1^+}$ and $M_{H_2^+}$ in Type-II 3HDM.

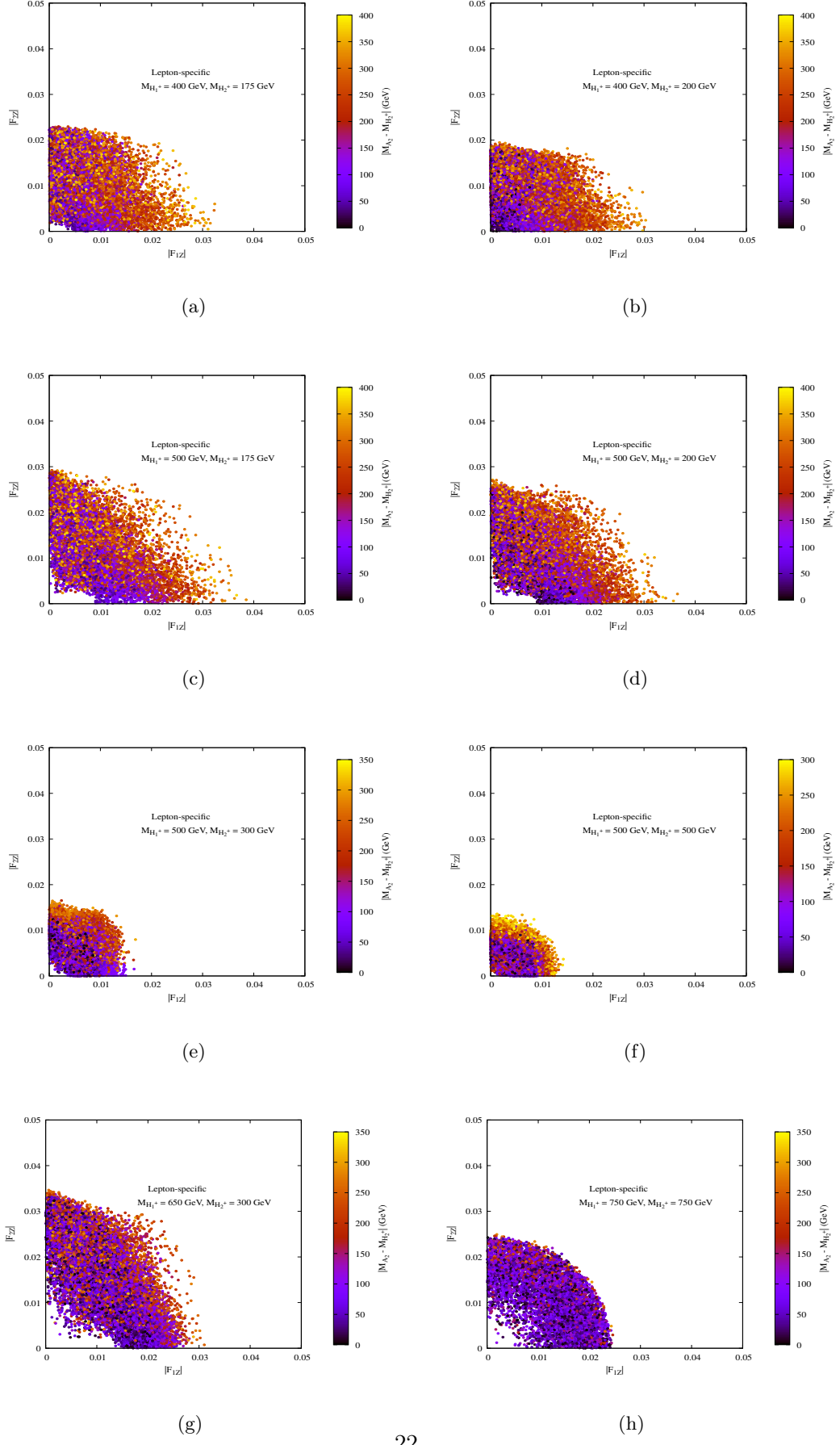


FIG. 7: $|F_{2Z}|$ vs. $|F_{1Z}|$ plots for different values of $M_{H_1^+}$ and $M_{H_2^+}$ in lepton-specific 3HDM.

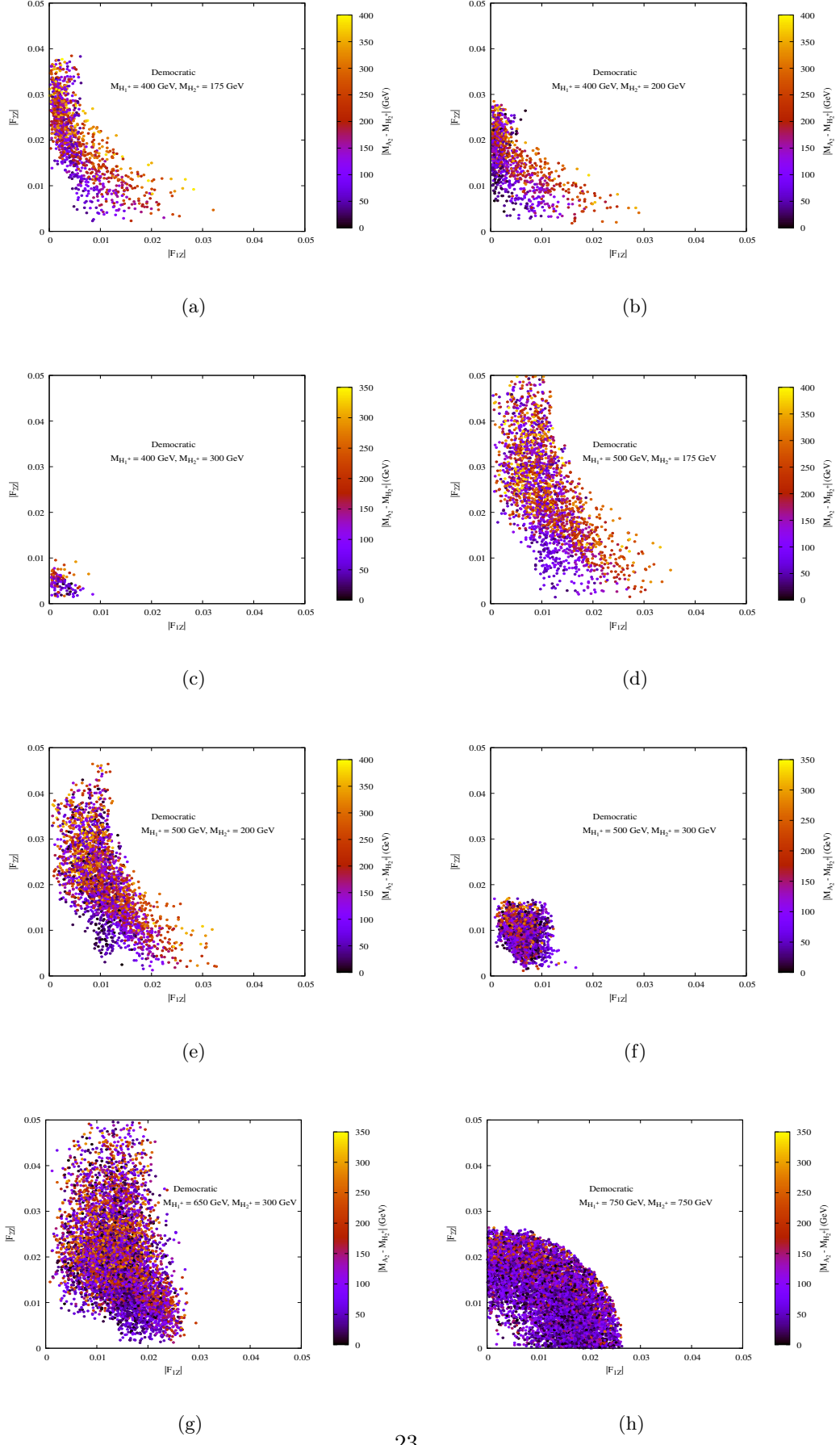


FIG. 8: $|F_{2Z}|$ vs. $|F_{1Z}|$ plots for different values of $M_{H_1^+}$ and $M_{H_2^+}$ in Democratic 3HDM.

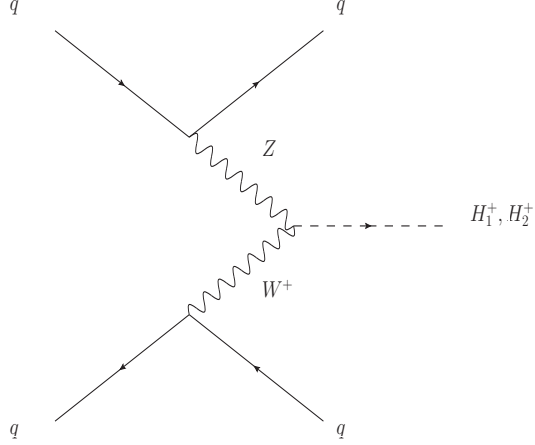


FIG. 9:

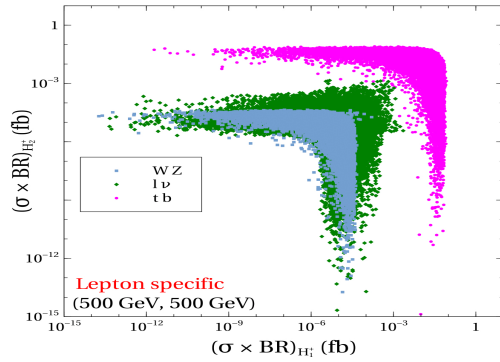
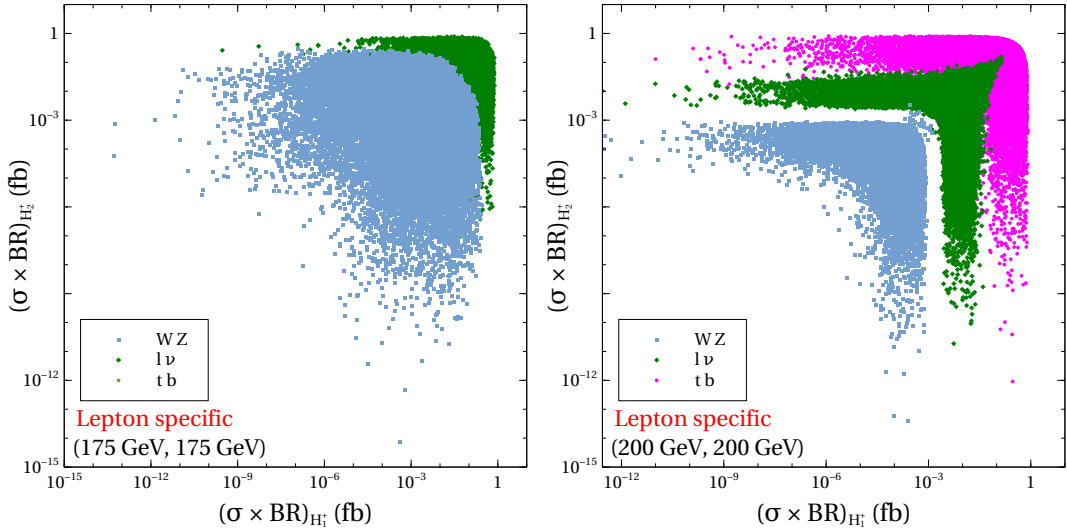


FIG. 10: $\sigma \times BR$ values for H_1^+ and H_2^+ . The color coding is shown in the legends.

Higgs masses. This is ascertained in case of $M_{H_1^+} = M_{H_2^+} = 500$ GeV wherein $pp \rightarrow H_{1,2}^\pm \rightarrow \tau\nu$ has a cross section not exceeding $\sim 10^{-3}$ fb. The main takeaway here is that charged Higgses with masses $\lesssim 200$ GeV can give rise to a $jj + \tau_h + \cancel{E}_T$ signature. This signature is interesting from the kinematic point of view given a single neutrino in the final state makes the charged Higgs mass potentially reconstructible. In addition, the event count at the pre-cut level can also be *gtrsim* 300 for an integrated luminosity $\mathcal{L} = 3000$ fb $^{-1}$.

Next, we study the prospects of $H_1^+ \rightarrow H_2^+ H_2$, $H_2^+ A_2$ modes. One notes that the leading fermionic decay mode for H_2 and A_2 is $\tau\bar{\tau}$ for the lepton-specific 3HDM whenever the $t\bar{t}$ threshold remains closed. In addition, taking the $H_2^+ \rightarrow \tau\nu$ decay implies that $pp \rightarrow H_1^\pm \rightarrow H_2^\pm H_2(A_2)$ can give rise to a $jj + 3\tau_h + \cancel{E}_T$ final state. The cross sections for the two aforesaid channels

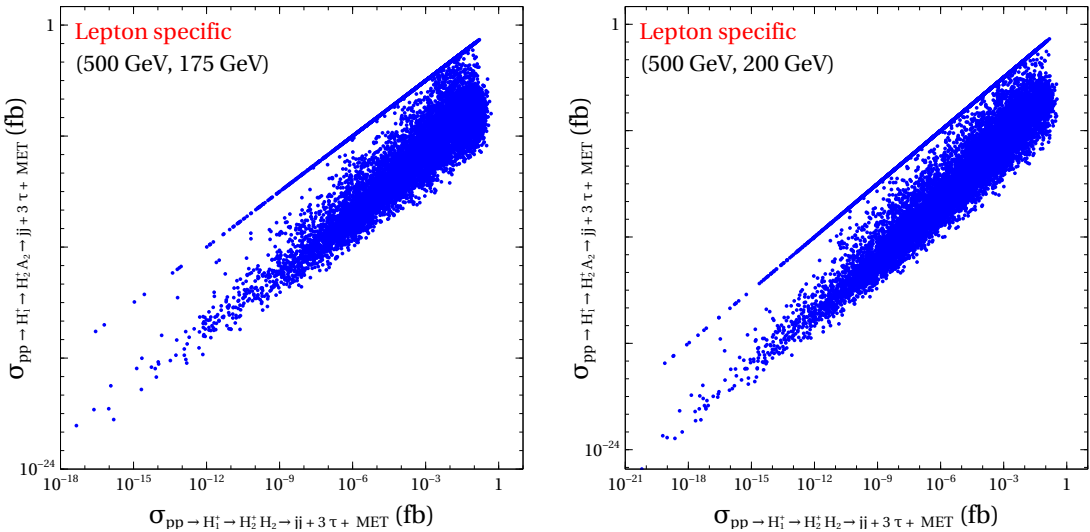


FIG. 11: $\sigma \times \text{BR}$ values for H_1^+ and H_2^+ . The color coding is shown in the legends.

are shown in Fig.11. A couple of comments are in order. First, $M_{H_2} = M_{H_2^+} = 175$ GeV, 200 GeV implies that $H_2 \rightarrow \tau\bar{\tau}$ is by far the most dominant mode. Secondly, A_2 is allowed to be heavier in our analysis and therefore $A_2 \rightarrow H_2 Z$, $H_2^\pm W^\mp$ also compete with $A_2 \rightarrow \tau\bar{\tau}$. Overall, the $jj + 3\tau_h + \cancel{E}_T$ originating from H_2 is seen to have a cross section $\sim \mathcal{O}(0.1 \text{ fb})$ despite the multiple cascades involved. The corresponding event count can be ~ 300 . More importantly, such a signal is kinematically rich and gives the scope to reconstruct both charged Higgs masses thereby being a potential smoking gun of a 3HDM.

VII. SUMMARY AND CONCLUSIONS

The weak isospin symmetry of the kinetic terms in multi-Higgs doublet models disallows H^+W^-Z interactions at the tree level. However, isospin-breaking effects stemming from the scalar and Yukawa sectors generate this vertex at the one-loop level. It is therefore interesting to estimate the size of this vertex in such models and probe its observability at the energy frontier. In this study, we have quantified the strength of the $H_{1,2}^+W^-Z$ vertices for flavour conserving 3HDMs. And we have chosen the Type-II, lepton specific and democratic Yukawa structures for illustration. Given the large number of one-loop diagrams, we have arranged them into UV-finite and gauge invariant subsets tagged by the scalar trilinear coupling involved. For a prototype subset, UV-finiteness is explicitly checked for and a numerical validation of Ward identity for the $H_1^+W^- \gamma$ amplitude is carried out as a check of gauge invariance.

It is observed that demanding appropriate relations between mixing angles in the scalar sector and scalar masses renders $\Delta T = 0$ thereby making the 3HDM parameter space easier to handle numerically. In addition, we have also pointed out that such relations crucially help segregate the excess contribution to the one-loop form factors over and above the 2HDM. We have folded in constraints coming from perturbative unitarity, Higgs to diphoton decay and $B \rightarrow X_s \gamma$ branching ratio in the ensuing scans and computed the one-loop form factors for the surviving parameter points. As a highlight of the numerical results, F_{1Z} and F_{2Z} for the lepton specific 3HDM can be $\simeq 0.045$ and $\simeq 0.03$ for $(M_{H_1^+}, M_{H_2^+}) = (500 \text{ GeV}, 200 \text{ GeV})$ respectively, a value sizeably enhanced compared to the $\simeq 0.01$ reported for 2HDMs.

We have also explored the possibility of probing the $H_{1,2}^+W^-Z$ vertices at the 14 TeV LHC through WZ fusion. The bare $\sigma \times \text{BR}$ values are estimated for $pp \times H_{1,2}^\pm$ with $H_{1,2}^+ \rightarrow tb$, $\tau\nu$, W^+Z for the 3HDM types taken. The lepton specific 3HDM fares particularly well in the $H_{1,2}^+ \rightarrow \tau\nu$ channel given the enhanced leptonic Yukawas. The $\sigma \times \text{BR}$ value can be $\sim 0.1 \text{ fb}$ in this case leading to $\mathcal{O}(100)$ events for an integrated luminosity 3000 fb^{-1} , modulo kinematical cuts. On the kinematic side, that there is a single neutrino in the signal makes the charged Higgs mass fully reconstructible for this signal. In addition to the above, the lepton specific 3HDM is also shown to accommodate $H_1^+ \rightarrow H_2^+ H_2$ with a sizeable branching ratio. With $H_2^+ \rightarrow \tau\nu$ and $H_2 \rightarrow \tau\tau$, one can obtain a $jj + 3\tau_h + \cancel{E}_T$ final state if the hadronic decays of τ are tagged. This signal therefore gives a scope to reconstruct the masses of both H_1^+ and H_2^+ up to τ_h combinatorics thereby being a potential smoking gun signature of a 3HDM. Moreover, a $\sigma \times \text{BR}$ value is $\sim 0.1 \text{ fb}$ makes it comparable to the $pp \rightarrow H_{1,2}^+ jj \rightarrow \tau jj + \cancel{E}_T$ in terms of event yield.

VIII. ACKNOWLEDGEMENTS

IC acknowledges support from Department of Science and Technology, Govt. of India, under grant number IFA18-PH214 (INSPIRE Faculty Award). NC acknowledges support from Department of Science and Technology, Govt. of India, under grant number IFA19-PH237 (INSPIRE Faculty Award). NC also thanks Arani Chakravarti for an useful computational help.

IX. APPENDIX

A. Scalar squared mass matrices

$$\begin{aligned}
 (M_{\text{even}}^2)_{11} &= \frac{\lambda_1 v_1^3 + m_{12}^2 v_2 + m_{13}^2 v_3}{v_1} \\
 (M_{\text{even}}^2)_{12} &= v_1 v_2 (\lambda_{12} + \lambda'_{12} + \lambda''_{12}) - m_{12}^2 \\
 (M_{\text{even}}^2)_{13} &= v_1 v_3 (\lambda_{13} + \lambda'_{13} + \lambda''_{13}) - m_{13}^2 \\
 (M_{\text{even}}^2)_{22} &= \frac{\lambda_2 v_2^3 + m_{12}^2 v_1 + m_{23}^2 v_3}{v_2} \\
 (M_{\text{even}}^2)_{23} &= v_2 v_3 (\lambda_{23} + \lambda'_{23} + \lambda''_{23}) - m_{23}^2 \\
 (M_{\text{even}}^2)_{33} &= \frac{\lambda_3 v_3^3 + m_{13}^2 v_1 + m_{23}^2 v_2}{v_3}
 \end{aligned} \tag{27a}$$

$$\begin{aligned}
 (M_{\text{odd}}^2)_{11} &= \frac{-\lambda''_{12} v_1 v_2^2 + v_3 (m_{13}^2 - \lambda''_{13} v_1 v_3) + m_{12}^2 v_2}{v_1} \\
 (M_{\text{odd}}^2)_{12} &= -m_{12}^2 + \lambda''_{12} v_1 v_2 \\
 (M_{\text{odd}}^2)_{13} &= -m_{13}^2 + \lambda''_{13} v_1 v_3 \\
 (M_{\text{odd}}^2)_{22} &= \frac{m_{12}^2 v_1 - \lambda''_{12} v_1^2 v_2 + v_3 (m_{23}^2 - \lambda''_{23} v_2 v_3)}{v_2} \\
 (M_{\text{odd}}^2)_{23} &= -m_{23}^2 + \lambda''_{23} v_2 v_3 \\
 (M_{\text{odd}}^2)_{33} &= \frac{m_{13}^2 v_1 + m_{23}^2 v_2 - (\lambda''_{13} v_1^2 + \lambda''_{23} v_2^2) v_3}{v_3}
 \end{aligned} \tag{28a}$$

$$\begin{aligned}
(M_{\text{ch}}^2)_{11} &= -\frac{-2m_{12}^2 v_2 + (\lambda'_{12} + \lambda''_{12}) v_1 v_2^2 - 2m_{13}^2 v_3 + (\lambda'_{13} + \lambda''_{13}) v_1 v_3^2}{2v_1} \\
(M_{\text{ch}}^2)_{12} &= -m_{12}^2 + \frac{1}{2}(\lambda'_{12} + \lambda''_{12}) v_1 v_2 \\
(M_{\text{ch}}^2)_{13} &= -m_{13}^2 + \frac{1}{2}(\lambda'_{13} + \lambda''_{13}) v_1 v_3 \\
(M_{\text{ch}}^2)_{22} &= -\frac{-2m_{12}^2 v_1 + (\lambda'_{12} + \lambda''_{12}) v_1 v_2^2 - 2m_{23}^2 v_3 + (\lambda'_{23} + \lambda''_{23}) v_2 v_3^2}{2v_2} \\
(M_{\text{ch}}^2)_{23} &= -m_{23}^2 + \frac{1}{2}(\lambda'_{23} + \lambda''_{23}) v_2 v_3 \\
(M_{\text{ch}}^2)_{33} &= \frac{2m_{13}^2 v_1 - (\lambda'_{13} + \lambda''_{13}) v_1^2 v_3 + 2m_{23}^2 v_2 - (\lambda'_{23} + \lambda''_{23}) v_2^2 v_3}{2v_3}
\end{aligned} \tag{29a}$$

B. One-loop diagrams

1. E-type amplitudes

Diagram number	F_Z
E_1	$\frac{1}{16\pi^2 v} \frac{s_W^2}{c_W} c_{\alpha_3+\delta_2} \lambda_{H_1^+ H_1^- H_1} B_0(q^2, H_1^+, H_1)$
E_2	$\frac{1}{16\pi^2 v} \frac{s_W^2}{c_W} s_{\alpha_3+\delta_2} \lambda_{H_1^+ H_2^- H_1} B_0(q^2, H_2^+, H_1)$
E_3	$-\frac{1}{16\pi^2 v} \frac{s_W^2}{c_W} s_{\alpha_3+\delta_2} \lambda_{H_1^+ H_1^- H_2} B_0(q^2, H_1^+, H_2)$
E_4	$\frac{1}{16\pi^2 v} \frac{s_W^2}{c_W} c_{\alpha_3+\delta_2} \lambda_{H_1^+ H_2^- H_2} B_0(q^2, H_2^+, H_2)$
E_5	$\frac{1}{16\pi^2 v} \frac{s_W^2}{c_W} c_{\alpha_3+\delta_2} \lambda_{H_2^+ H_1^- H_1} B_0(q^2, H_1^+, H_1)$
E_6	$\frac{1}{16\pi^2 v} \frac{s_W^2}{c_W} s_{\alpha_3+\delta_2} \lambda_{H_2^+ H_2^- H_1} B_0(q^2, H_2^+, H_1)$
E_7	$-\frac{1}{16\pi^2 v} \frac{s_W^2}{c_W} s_{\alpha_3+\delta_2} \lambda_{H_2^+ H_1^- H_2} B_0(q^2, H_1^+, H_2)$
E_8	$\frac{1}{16\pi^2 v} \frac{s_W^2}{c_W} c_{\alpha_3+\delta_2} \lambda_{H_2^+ H_2^- H_2} B_0(q^2, H_2^+, H_2)$

TABLE VI:

2. L-, M-, N-type amplitudes

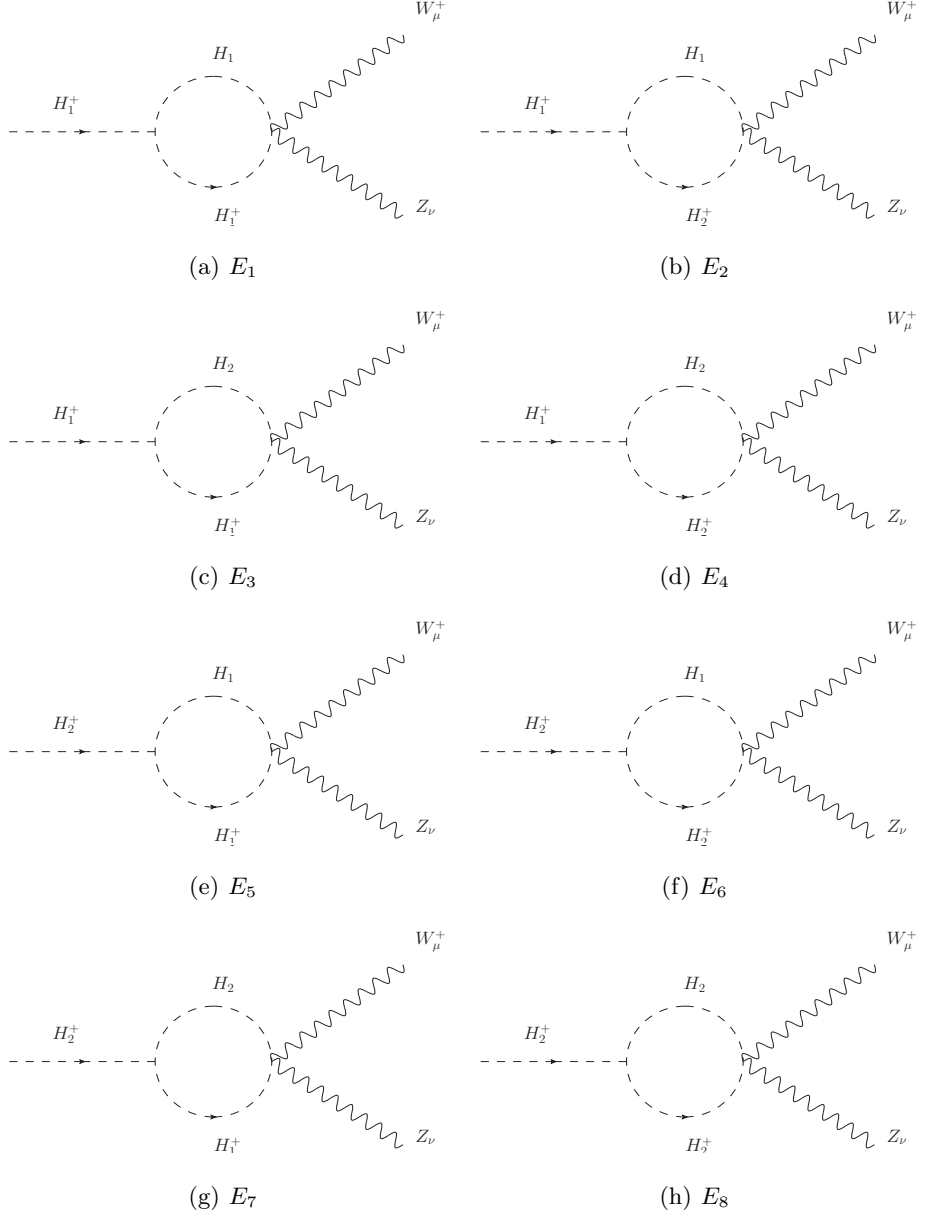


FIG. 12:

3. E' -type amplitudes

4. Fermionic diagrams

5. O -type amplitudes

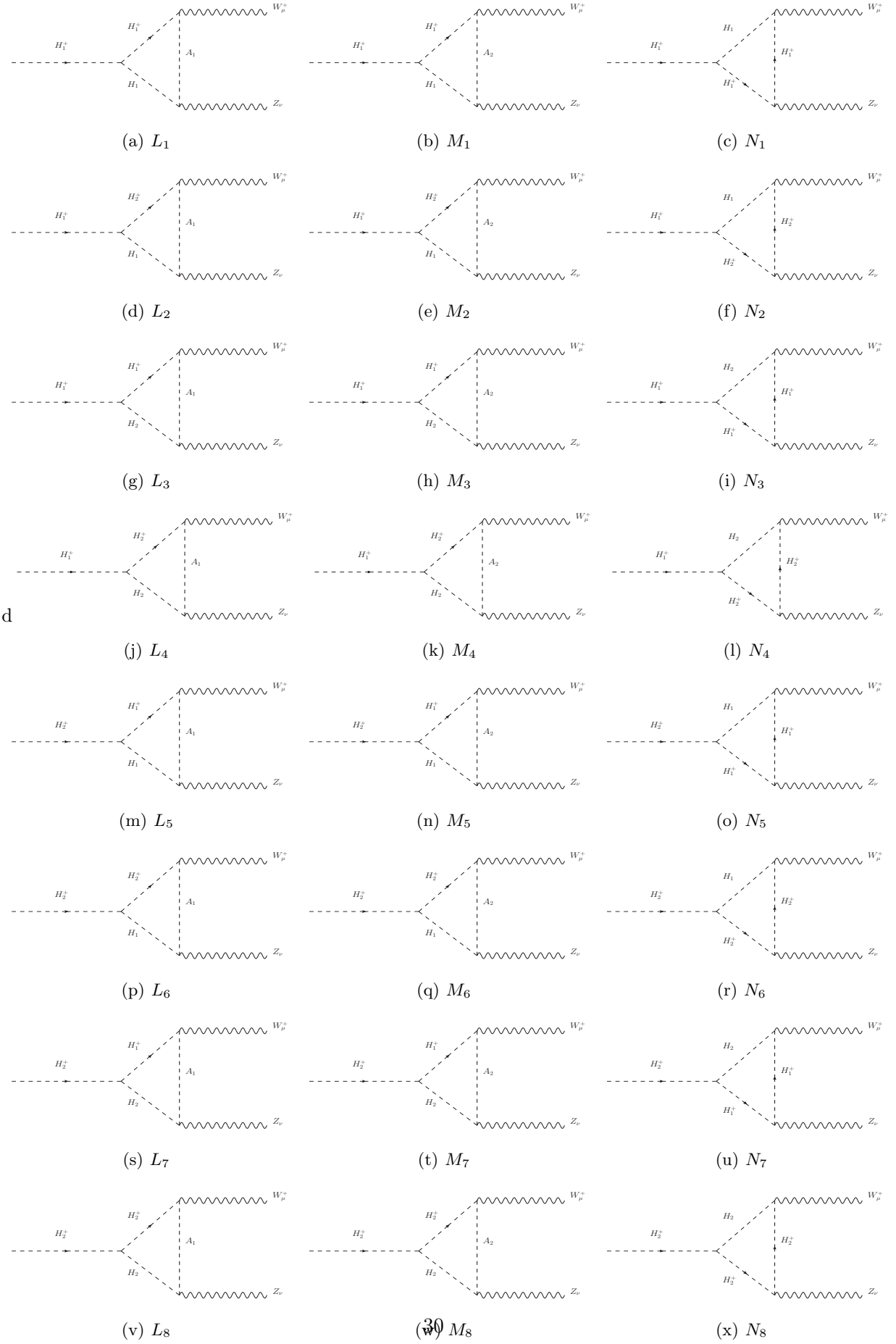


FIG. 13:

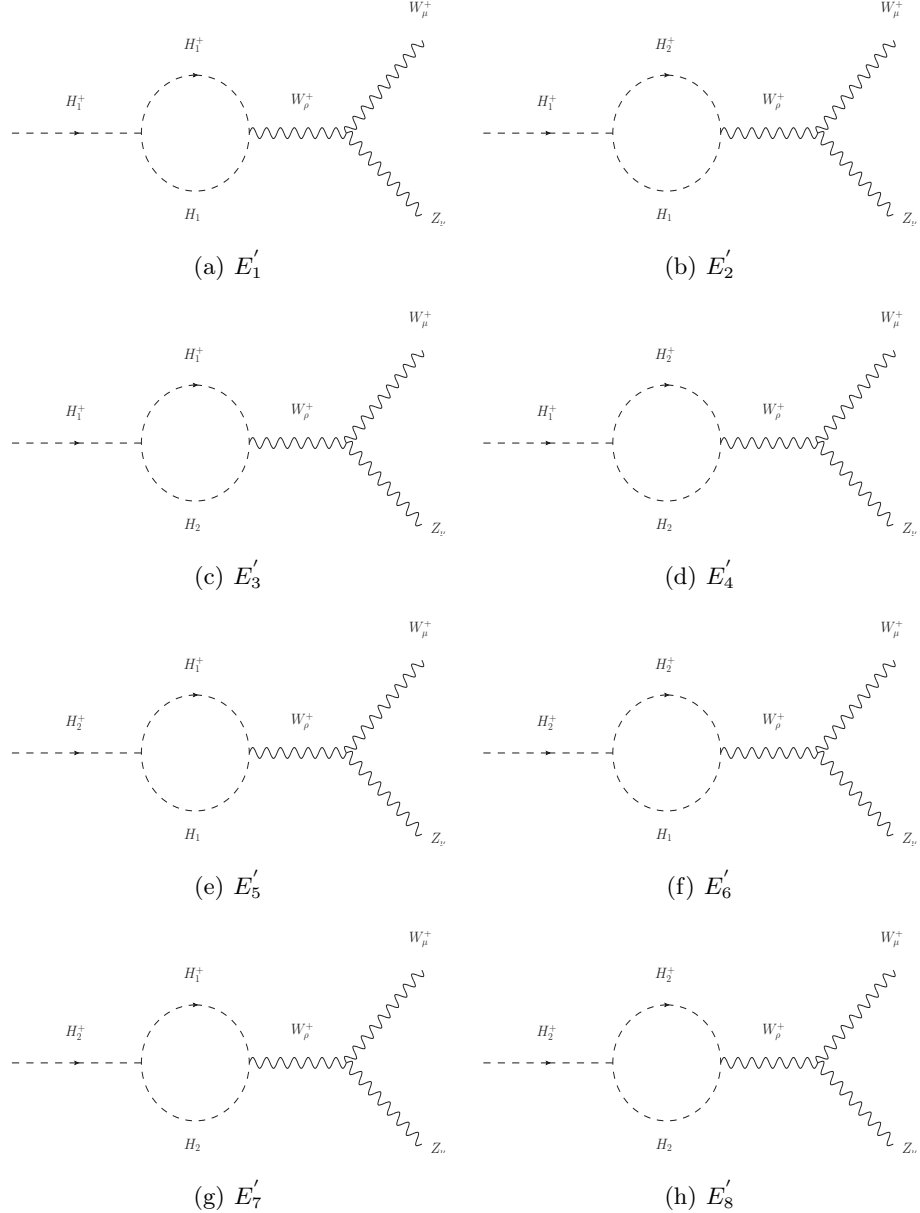


FIG. 14:

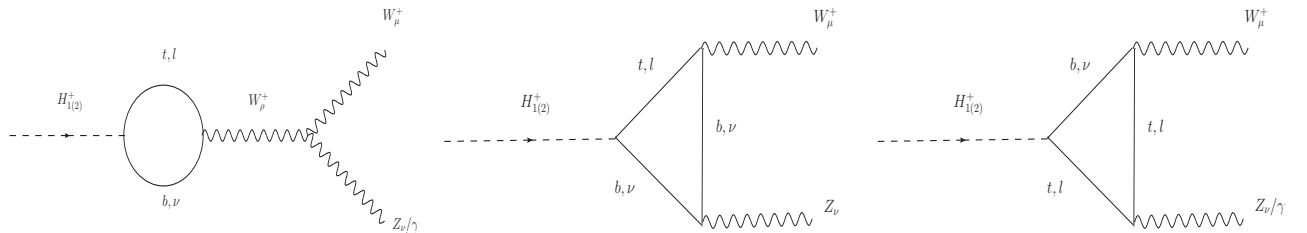


FIG. 15:

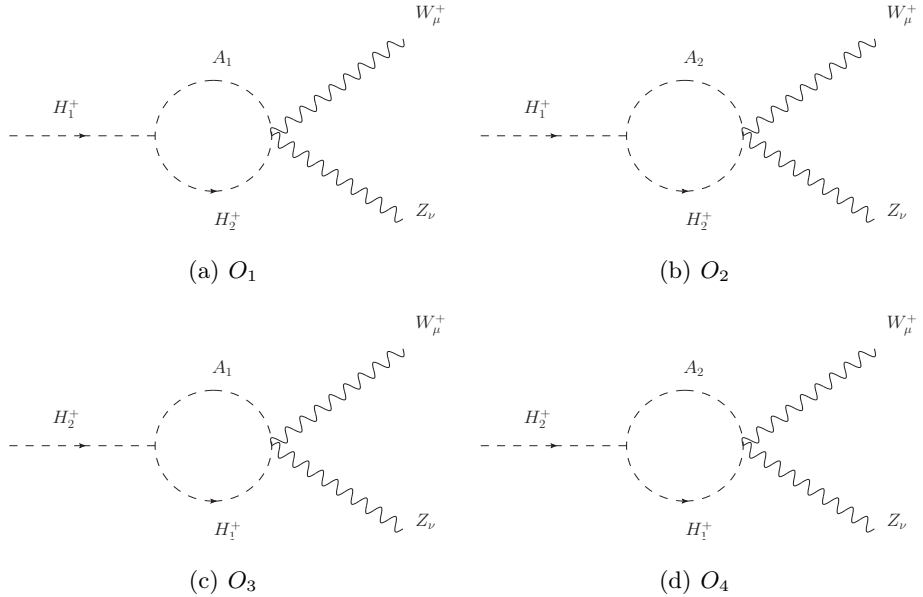


FIG. 16:

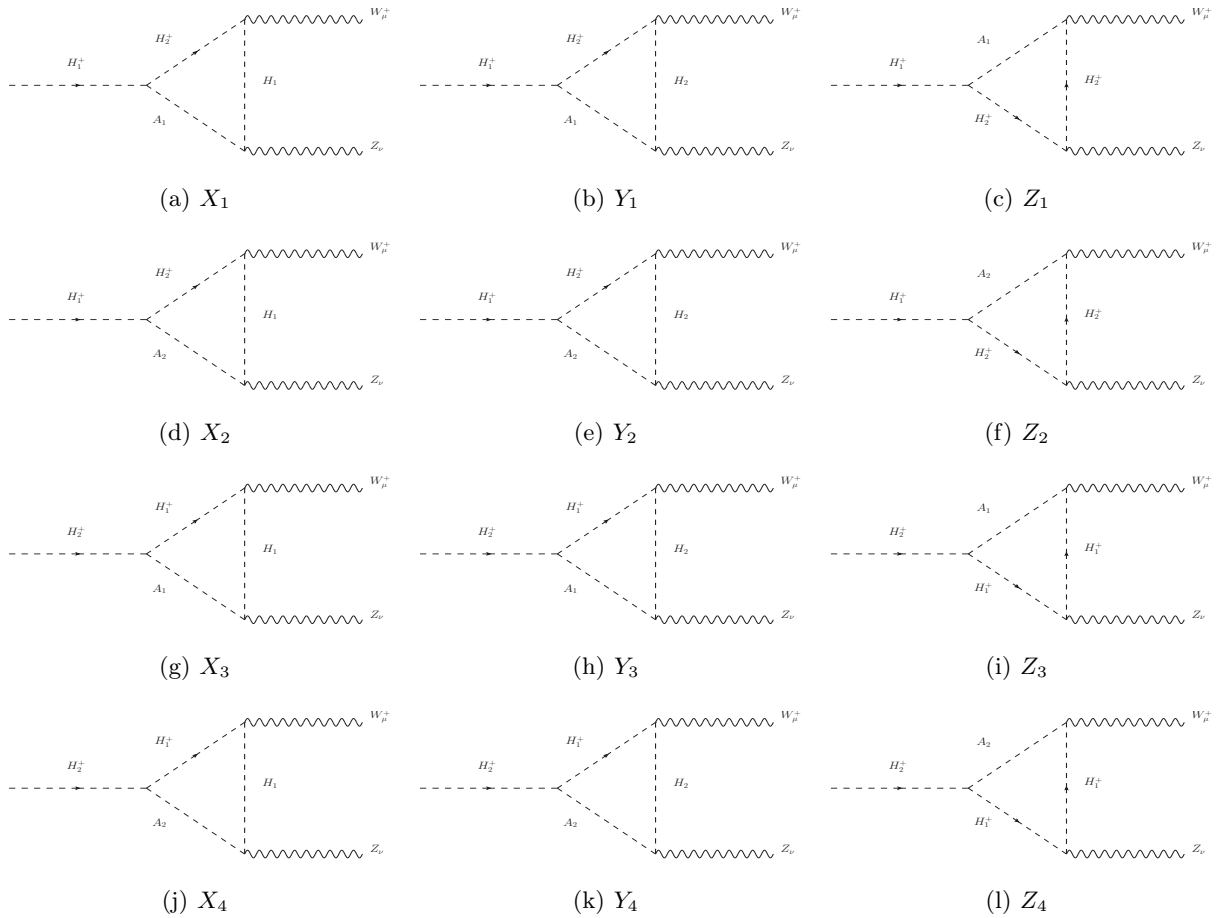


FIG. 17:

Diagram number	F_Z
E'_1	$\frac{1}{16\pi^2 v} \frac{s_W^2}{c_W} c_{\alpha_3+\delta_2} \lambda_{H_1^+ H_1^- H_1} [B_0(q^2, H_1^+, H_1) + 2B_1(q^2, H_1^+, H_1)]$
E'_2	$\frac{1}{16\pi^2 v} \frac{s_W^2}{c_W} s_{\alpha_3+\delta_2} \lambda_{H_1^+ H_2^- H_1} [B_0(q^2, H_2^+, H_1) + 2B_1(q^2, H_2^+, H_1)]$
E'_3	$-\frac{1}{16\pi^2 v} \frac{s_W^2}{c_W} s_{\alpha_3+\delta_2} \lambda_{H_1^+ H_1^- H_2} [B_0(q^2, H_1^+, H_2) + 2B_1(q^2, H_1^+, H_2)]$
E'_4	$\frac{1}{16\pi^2 v} \frac{s_W^2}{c_W} c_{\alpha_3+\delta_2} \lambda_{H_1^+ H_2^- H_2} [B_0(q^2, H_2^+, H_2) + 2B_1(q^2, H_2^+, H_2)]$
E'_5	$\frac{1}{16\pi^2 v} \frac{s_W^2}{c_W} c_{\alpha_3+\delta_2} \lambda_{H_2^+ H_1^- H_1} [B_0(q^2, H_1^+, H_1) + 2B_1(q^2, H_1^+, H_1)]$
E'_6	$\frac{1}{16\pi^2 v} \frac{s_W^2}{c_W} s_{\alpha_3+\delta_2} \lambda_{H_2^+ H_2^- H_1} [B_0(q^2, H_2^+, H_1) + 2B_1(q^2, H_2^+, H_1)]$
E'_7	$-\frac{1}{16\pi^2 v} \frac{s_W^2}{c_W} s_{\alpha_3+\delta_2} \lambda_{H_2^+ H_1^- H_2} [B_0(q^2, H_1^+, H_2) + 2B_1(q^2, H_1^+, H_2)]$
E'_8	$\frac{1}{16\pi^2 v} \frac{s_W^2}{c_W} c_{\alpha_3+\delta_2} \lambda_{H_2^+ H_2^- H_2} [B_0(q^2, H_2^+, H_2) + 2B_1(q^2, H_2^+, H_2)]$

TABLE VIII:

Diagram number	F_Z
O_1	$-\frac{1}{16\pi^2 v} \frac{s_W^2}{c_W} s_{\delta_1-\delta_2} \lambda_{H_1^+ H_2^- A_1} B_0(q^2, H_2^+, A_1)$
O_2	$\frac{1}{16\pi^2 v} \frac{s_W^2}{c_W} c_{\delta_1-\delta_2} \lambda_{H_1^+ H_2^- A_2} B_0(q^2, H_2^+, A_2)$
O_3	$\frac{1}{16\pi^2 v} \frac{s_W^2}{c_W} c_{\delta_1-\delta_2} \lambda_{H_2^+ H_1^- A_1} B_0(q^2, H_1^+, A_1)$
O_4	$\frac{1}{16\pi^2 v} \frac{s_W^2}{c_W} s_{\delta_1-\delta_2} \lambda_{H_2^+ H_1^- A_2} B_0(q^2, H_1^+, A_2)$

TABLE IX: Corrected table

Diagram no.	F_Z	G_Z
X_1	$\left(-\frac{2\lambda_{H_1^+ H_2^- A_1}}{16\pi^2 v c_W}\right) (s_{\alpha_3+\delta_2} c_{\alpha_3+\delta_1}) C_{24}(H_2^+, H_1, A_1)$	$\left(-\frac{2\lambda_{H_1^+ H_2^- A_1}}{16\pi^2 v c_W}\right) M_W^2 (s_{\alpha_3+\delta_2} c_{\alpha_3+\delta_1}) C_{1223}(H_2^+, H_1, A_1)$
Y_1	$\left(-\frac{2\lambda_{H_1^+ H_2^- A_1}}{16\pi^2 v c_W}\right) (-c_{\alpha_3+\delta_2} s_{\alpha_3+\delta_1}) C_{24}(H_2^+, H_2, A_1)$	$\left(-\frac{2\lambda_{H_1^+ H_2^- A_1}}{16\pi^2 v c_W}\right) M_W^2 (-c_{\alpha_3+\delta_2} s_{\alpha_3+\delta_1}) C_{1223}(H_2^+, H_2, A_1)$
Z_1	$(-\frac{2c_{2W}}{c_W}) \frac{\lambda_{H_1^+ H_2^- A_1}}{16\pi^2 v} s_{\delta_1-\delta_2} C_{24}(A_1, H_2^+, H_2^+)$	$(-\frac{2c_{2W}}{c_W}) \frac{\lambda_{H_1^+ H_2^- A_1}}{16\pi^2 v} M_W^2 s_{\delta_1-\delta_2} C_{1223}(A_1, H_2^+, H_2^+)$
X_2	$\left(-\frac{2\lambda_{H_1^+ H_2^- A_2}}{16\pi^2 v c_W}\right) (s_{\alpha_3+\delta_2} s_{\alpha_3+\delta_1}) C_{24}(H_2^+, H_1, A_2)$	$\left(-\frac{2\lambda_{H_1^+ H_2^- A_2}}{16\pi^2 v c_W}\right) M_W^2 (s_{\alpha_3+\delta_2} s_{\alpha_3+\delta_1}) C_{1223}(H_2^+, H_1, A_2)$
Y_2	$\left(-\frac{2\lambda_{H_1^+ H_2^- A_2}}{16\pi^2 v c_W}\right) (c_{\alpha_3+\delta_2} c_{\alpha_3+\delta_1}) C_{24}(H_2^+, H_2, A_2)$	$\left(-\frac{2\lambda_{H_1^+ H_2^- A_2}}{16\pi^2 v c_W}\right) M_W^2 (c_{\alpha_3+\delta_2} c_{\alpha_3+\delta_1}) C_{1223}(H_2^+, H_2, A_2)$
Z_2	$(\frac{2c_{2W}}{c_W}) \frac{\lambda_{H_1^+ H_2^- A_2}}{16\pi^2 v} c_{\delta_1-\delta_2} C_{24}(A_2, H_2^+, H_2^+)$	$(\frac{2c_{2W}}{c_W}) \frac{\lambda_{H_1^+ H_2^- A_2}}{16\pi^2 v} M_W^2 c_{\delta_1-\delta_2} C_{1223}(A_2, H_2^+, H_2^+)$
X_3	$\left(-\frac{2\lambda_{H_2^+ H_1^- A_1}}{16\pi^2 v c_W}\right) (c_{\alpha_3+\delta_2} c_{\alpha_3+\delta_1}) C_{24}(H_1^+, H_1, A_1)$	$\left(-\frac{2\lambda_{H_2^+ H_1^- A_1}}{16\pi^2 v c_W}\right) M_W^2 (c_{\alpha_3+\delta_2} c_{\alpha_3+\delta_1}) C_{1223}(H_1^+, H_1, A_1)$
Y_3	$\left(-\frac{2\lambda_{H_2^+ H_1^- A_1}}{16\pi^2 v c_W}\right) (s_{\alpha_3+\delta_2} s_{\alpha_3+\delta_1}) C_{24}(H_1^+, H_2, A_1)$	$\left(-\frac{2\lambda_{H_2^+ H_1^- A_1}}{16\pi^2 v c_W}\right) M_W^2 (s_{\alpha_3+\delta_2} s_{\alpha_3+\delta_1}) C_{1223}(H_1^+, H_2, A_1)$
Z_3	$(\frac{2c_{2W}}{c_W}) \frac{\lambda_{H_2^+ H_1^- A_1}}{16\pi^2 v} c_{\delta_1-\delta_2} C_{24}(A_1, H_1^+, H_1^+)$	$(\frac{2c_{2W}}{c_W}) \frac{\lambda_{H_2^+ H_1^- A_1}}{16\pi^2 v} M_W^2 c_{\delta_1-\delta_2} C_{1223}(A_1, H_1^+, H_1^+)$
X_4	$\left(-\frac{2\lambda_{H_2^+ H_1^- A_2}}{16\pi^2 v c_W}\right) (c_{\alpha_3+\delta_2} s_{\alpha_3+\delta_1}) C_{24}(H_1^+, H_1, A_2)$	$\left(-\frac{2\lambda_{H_2^+ H_1^- A_2}}{16\pi^2 v c_W}\right) M_W^2 (c_{\alpha_3+\delta_2} s_{\alpha_3+\delta_1}) C_{1223}(H_1^+, H_1, A_2)$
Y_4	$\left(-\frac{2\lambda_{H_2^+ H_1^- A_2}}{16\pi^2 v c_W}\right) (-s_{\alpha_3+\delta_2} c_{\alpha_3+\delta_1}) C_{24}(H_1^+, H_2, A_2)$	$\left(-\frac{2\lambda_{H_2^+ H_1^- A_2}}{16\pi^2 v c_W}\right) M_W^2 (-s_{\alpha_3+\delta_2} c_{\alpha_3+\delta_1}) C_{1223}(H_1^+, H_2, A_2)$
Z_4	$(\frac{2c_{2W}}{c_W}) \frac{\lambda_{H_2^+ H_1^- A_2}}{16\pi^2 v} s_{\delta_1-\delta_2} C_{24}(A_2, H_1^+, H_1^+)$	$(\frac{2c_{2W}}{c_W}) \frac{\lambda_{H_2^+ H_1^- A_2}}{16\pi^2 v} M_W^2 s_{\delta_1-\delta_2} C_{1223}(A_2, H_1^+, H_1^+)$

TABLE X: Corrected table

7. O' -type amplitudes

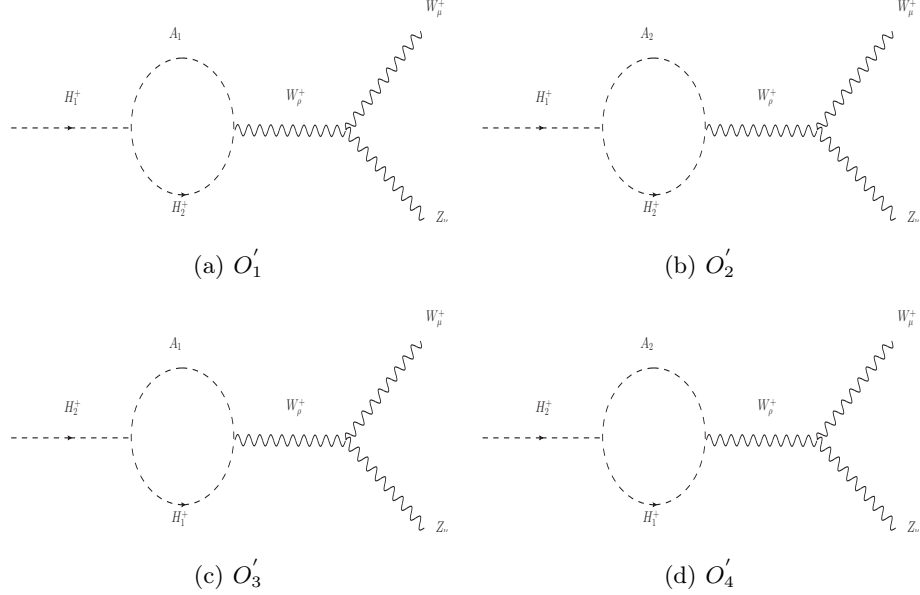


FIG. 18:

Diagram number	F_Z
O'_1	$-\frac{1}{16\pi^2 v} \frac{s_W^2}{c_W} s_{\delta_1-\delta_2} \lambda_{H_1^+ H_2^- A_1} [B_0(q^2, H_2^+, A_1) + 2B_1(q^2, H_2^+, A_1)]$
O'_2	$\frac{1}{16\pi^2 v} \frac{s_W^2}{c_W} c_{\delta_1-\delta_2} \lambda_{H_1^+ H_2^- A_2} [B_0(q^2, H_2^+, A_2) + 2B_1(q^2, H_2^+, A_2)]$
O'_3	$\frac{1}{16\pi^2 v} \frac{s_W^2}{c_W} c_{\delta_1-\delta_2} \lambda_{H_2^+ H_1^- A_1} [B_0(q^2, H_1^+, A_1) + 2B_1(q^2, H_1^+, A_1)]$
O'_4	$\frac{1}{16\pi^2 v} \frac{s_W^2}{c_W} s_{\delta_1-\delta_2} \lambda_{H_2^+ H_1^- A_2} [B_0(q^2, H_1^+, A_2) + 2B_1(q^2, H_1^+, A_2)]$

TABLE XI:

C. Passarino-Veltman functions

$$B_0(p^2; M_1^2, M_2^2) = \int \frac{d^d k}{i\pi^2} \frac{1}{(k^2 - M_1^2)((k+p)^2 - M_2^2)}, \quad (30a)$$

$$p^\mu B_1(p^2; M_1^2, M_2^2) = \int \frac{d^d k}{i\pi^2} \frac{k^\mu}{(k^2 - M_1^2)((k+p)^2 - M_2^2)}. \quad (30b)$$

We also have

$$\begin{aligned} & C_0(p_1^2, p_2^2, q^2; M_1^2, M_2^2, M_3^2) \\ &= \int \frac{d^d k}{i\pi^2} \frac{1}{(k^2 - M_1^2)((k+p_1)^2 - M_2^2)(k+q)^2 - M_3^2} \end{aligned} \quad (31a)$$

$$\begin{aligned} & (p_1^\mu C_{11} + p_2^\mu C_{12})(p_1^2, p_2^2, q^2; M_1^2, M_2^2, M_3^2) \\ &= \int \frac{d^d k}{i\pi^2} \frac{k^\mu}{(k^2 - M_1^2)((k+p_1)^2 - M_2^2)(k+q)^2 - M_3^2} \end{aligned} \quad (31b)$$

$$\begin{aligned} & (p_1^\mu p_1^\nu C_{21} + p_2^\mu p_2^\nu C_{22} + p_1^\mu p_2^\nu C_{23} + g^{\mu\nu} C_{24})(p_1^2, p_2^2, q^2; M_1^2, M_2^2, M_3^2) \\ &= \int \frac{d^d k}{i\pi^2} \frac{k^\mu k^\nu}{(k^2 - M_1^2)((k+p_1)^2 - M_2^2)(k+q)^2 - M_3^2} \end{aligned} \quad (31c)$$

The Passarino-Veltman functions are expressed in terms of the Feynman parameter integrals as

$$B_0(p^2; M_1^2, M_2^2) = \text{div} - \int_0^1 dx \ln \Delta_B, \quad (32a)$$

$$B_1(p^2; M_1^2, M_2^2) = -\frac{\text{div}}{2} + \int_0^1 dx (1-x) \ln \Delta_B, \quad (32b)$$

$$C_0(p_1^2, p_2^2, q^2; M_1^2, M_2^2, M_3^2) = - \int_0^1 dx \int_0^1 dy \frac{y}{\Delta_C}, \quad (32c)$$

$$C_{11}(p_1^2, p_2^2, q^2; M_1^2, M_2^2, M_3^2) = - \int_0^1 dx \int_0^1 dy \frac{y(xy-1)}{\Delta_C}, \quad (32d)$$

$$C_{12}(p_1^2, p_2^2, q^2; M_1^2, M_2^2, M_3^2) = - \int_0^1 dx \int_0^1 dy \frac{y(y-1)}{\Delta_C}, \quad (32e)$$

$$C_{21}(p_1^2, p_2^2, q^2; M_1^2, M_2^2, M_3^2) = - \int_0^1 dx \int_0^1 dy \frac{y(1-xy)^2}{\Delta_C}, \quad (32f)$$

$$C_{22}(p_1^2, p_2^2, q^2; M_1^2, M_2^2, M_3^2) = - \int_0^1 dx \int_0^1 dy \frac{y(1-y)^2}{\Delta_C}, \quad (32g)$$

$$C_{23}(p_1^2, p_2^2, q^2; M_1^2, M_2^2, M_3^2) = - \int_0^1 dx \int_0^1 dy \frac{y(1-xy)(1-y)}{\Delta_C}, \quad (32h)$$

$$C_{24}(p_1^2, p_2^2, q^2; M_1^2, M_2^2, M_3^2) = \frac{\text{div}}{4} - \frac{1}{2} \int_0^1 dx \int_0^1 dy y \ln \Delta_C. \quad (32i)$$

Where,

$$\Delta_B = -x(1-x)p^2 + xM_1^2 + (1-x)M_2^2, \quad (33a)$$

$$\Delta_C = y^2(p_1x + p_2)^2 + y[x(p_2^2 - q^2 + M_1^2 - M_2^2) + M_2^2 - M_3^2 - p_2^2] + M_3^2. \quad (33b)$$

D. Perturbative unitarity

This approach is based on the conservation of the total weak isospin σ and total hypercharge Y in the high energy scalar-scalar scattering. In addition, the incoming and outgoing states should remain invariant under the discrete symmetry $\mathbb{Z}_2 \times \mathbb{Z}'_2 \times \mathbb{Z}''_2$ originally present in the scalar potential. The states acquire following different combinations which are either even or odd under the aforesaid symmetry : $(+++), (- - +), (+ - -)$ and $(- + -)$. We construct several scalar-scalar states out of the charged fields ω_i^\pm and neutral fields n_i, n_i^* and tabulate them according to the weak isospin and its z -projection σ_z , hypercharge and $\mathbb{Z}_2 \times \mathbb{Z}'_2 \times \mathbb{Z}''_2$ charge assignment. We have quoted the states with $Y = 2$ and $Y = 0$ in Table XII and Table XIII respectively. From Table XII, it can be seen that the $(+++)$ scattering state with $Y = 2, \sigma = 0$ is absent owing to the Bose-Einstein symmetry of the identical particles.

Y	σ	σ_z	$(+++)$	$(- - +)$	$(+ - -)$	$(- + -)$
2	1	1	$\begin{pmatrix} \omega_1^+ \omega_1^+ \\ \omega_2^+ \omega_2^+ \\ \omega_3^+ \omega_3^+ \end{pmatrix}$	$\omega_1^+ \omega_2^+$	$\omega_2^+ \omega_3^+$	$\omega_1^+ \omega_3^+$
		0	$\begin{pmatrix} \omega_1^+ n_1 \\ \omega_2^+ n_2 \\ \omega_3^+ n_3 \end{pmatrix}$	$\frac{\omega_1^+ n_2 + \omega_2^+ n_1}{\sqrt{2}}$	$\frac{\omega_2^+ n_3 + \omega_3^+ n_2}{\sqrt{2}}$	$\frac{\omega_1^+ n_3 + \omega_3^+ n_1}{\sqrt{2}}$
	-1		$\begin{pmatrix} n_1 n_1 \\ n_2 n_2 \\ n_3 n_3 \end{pmatrix}$	$n_1 n_2$	$n_2 n_3$	$n_1 n_3$
		0	absent	$\frac{(\omega_1^+ n_2 - \omega_2^+ n_1)}{\sqrt{2}}$	$\left(\begin{array}{c} \frac{\omega_1^+ \omega_1^+ + n_1 n_1^*}{\sqrt{2}} \\ \frac{\omega_2^+ \omega_2^+ + n_2 n_2^*}{\sqrt{2}} \end{array} \right)$	$\left(\begin{array}{c} \frac{\omega_1^+ \omega_2^- + n_1 n_2^*}{\sqrt{2}} \\ \frac{\omega_2^+ \omega_1^- + n_2 n_1^*}{\sqrt{2}} \end{array} \right)$

TABLE XII: Scalar-scalar scattering states with $Y = 2$.

Corresponding scattering matrices for different two-scalar states with different hypercharges, total weak isospin and $\mathbb{Z}_2 \times \mathbb{Z}'_2 \times \mathbb{Z}''_2$ charges are given in Table XIV. These scattering matrices do not depend on σ_z . The elements of the scattering matrices are computed by extracting the coefficients of the scattering states out of the scalar potential and folding them with appropriate symmetry factors. Next we calculate the eigenvalues of the scattering matrices e_i 's and put the bound as : $|e_i| \geq 8\pi$.

Y	σ	σ_z	(+ + +)	(- - +)	(+ - -)	(- + -)
0	1	1	$\begin{pmatrix} \omega_1^+ n_1^* \\ \omega_2^+ n_2^* \\ \omega_3^+ n_3^* \end{pmatrix}$	$\begin{pmatrix} \omega_1^+ n_2^* \\ \omega_2^+ n_1^* \end{pmatrix}$	$\begin{pmatrix} \omega_2^+ n_3^* \\ \omega_3^+ n_2^* \end{pmatrix}$	$\begin{pmatrix} \omega_1^+ n_3^* \\ \omega_3^+ n_1^* \end{pmatrix}$
		0	$\begin{pmatrix} \frac{\omega_1^+ \omega_1^+ - n_1 n_1^*}{\sqrt{2}} \\ \frac{\omega_2^+ \omega_2^+ - n_2 n_2^*}{\sqrt{2}} \\ \frac{\omega_3^+ \omega_3^+ - n_3 n_3^*}{\sqrt{2}} \end{pmatrix}$	$\begin{pmatrix} \frac{\omega_1^+ \omega_2^- - n_1 n_2^*}{\sqrt{2}} \\ \frac{\omega_2^+ \omega_1^- - n_2 n_1^*}{\sqrt{2}} \end{pmatrix}$	$\begin{pmatrix} \frac{\omega_2^+ \omega_3^- - n_2 n_3^*}{\sqrt{2}} \\ \frac{\omega_3^+ \omega_2^- - n_3 n_2^*}{\sqrt{2}} \end{pmatrix}$	$\begin{pmatrix} \frac{\omega_3^+ \omega_1^- - n_3 n_1^*}{\sqrt{2}} \\ \frac{\omega_1^+ \omega_3^- - n_1 n_3^*}{\sqrt{2}} \end{pmatrix}$
	-1	-1	$\begin{pmatrix} \omega_1^- n_1 \\ \omega_2^- n_2 \\ \omega_3^- n_3 \end{pmatrix}$	$\begin{pmatrix} \omega_1^- n_2 \\ \omega_2^- n_1 \end{pmatrix}$	$\begin{pmatrix} \omega_2^- n_3 \\ \omega_3^- n_2 \end{pmatrix}$	$\begin{pmatrix} \omega_3^- n_1 \\ \omega_1^- n_3 \end{pmatrix}$
		0	$\begin{pmatrix} \frac{\omega_1^+ \omega_1^+ + n_1 n_1^*}{\sqrt{2}} \\ \frac{\omega_2^+ \omega_2^+ + n_2 n_2^*}{\sqrt{2}} \\ \frac{\omega_3^+ \omega_3^+ + n_3 n_3^*}{\sqrt{2}} \end{pmatrix}$	$\begin{pmatrix} \frac{\omega_1^+ \omega_2^- + n_1 n_2^*}{\sqrt{2}} \\ \frac{\omega_2^+ \omega_1^- + n_2 n_1^*}{\sqrt{2}} \end{pmatrix}$	$\begin{pmatrix} \frac{\omega_2^+ \omega_3^- + n_2 n_3^*}{\sqrt{2}} \\ \frac{\omega_3^+ \omega_2^- + n_3 n_2^*}{\sqrt{2}} \end{pmatrix}$	$\begin{pmatrix} \frac{\omega_3^+ \omega_1^- + n_3 n_1^*}{\sqrt{2}} \\ \frac{\omega_1^+ \omega_3^- + n_1 n_3^*}{\sqrt{2}} \end{pmatrix}$

TABLE XIII: Scalar-scalar scattering states with $Y = 0$.

Y	σ	(+ + +)	(- - +)	(+ - -)	(- + -)
± 2	1	$\begin{pmatrix} \lambda_1 & \lambda_{12}'' & \lambda_{13}''' \\ \lambda_{12}'' & \lambda_2 & \lambda_{23}'' \\ \lambda_{13}''' & \lambda_{23}'' & \lambda_3 \end{pmatrix}$	$(\lambda_{12} + \lambda_{12}'')$	$(\lambda_{23} + \lambda_{23}'')$	$(\lambda_{13} + \lambda_{13}'')$
± 2	0	-	$(\lambda_{12} - \lambda_{12}'')$	$(\lambda_{23} - \lambda_{23}'')$	$(\lambda_{13} - \lambda_{13}'')$
0	1	$\begin{pmatrix} \lambda_1 & \lambda_{12}' & \lambda_{13}' \\ \lambda_{12}' & \lambda_2 & \lambda_{23}' \\ \lambda_{13}' & \lambda_{23}' & \lambda_3 \end{pmatrix}$	$\begin{pmatrix} \lambda_{12} & \lambda_{12}'' \\ \lambda_{12}'' & \lambda_{12} \end{pmatrix}$	$\begin{pmatrix} \lambda_{23} & \lambda_{23}'' \\ \lambda_{23}'' & \lambda_{23} \end{pmatrix}$	$\begin{pmatrix} \lambda_{13} & \lambda_{13}'' \\ \lambda_{13}'' & \lambda_{13} \end{pmatrix}$
0	0	$\begin{pmatrix} 3\lambda_1 & 2\lambda_{12} + \lambda_{12}' & 2\lambda_{13} + \lambda_{13}' \\ 2\lambda_{12} + \lambda_{12}' & 3\lambda_2 & 2\lambda_{23} + \lambda_{23}' \\ 2\lambda_{13} + \lambda_{13}' & 2\lambda_{23} + \lambda_{23}' & 3\lambda_3 \end{pmatrix}$	$\begin{pmatrix} \lambda_{12} + 2\lambda_{12}' & 3\lambda_{12}' \\ 3\lambda_{12}' & \lambda_{12} + 2\lambda_{12}' \end{pmatrix}$	$\begin{pmatrix} \lambda_{23} + 2\lambda_{23}'' & 3\lambda_{23}'' \\ 3\lambda_{23}'' & \lambda_{23} + 2\lambda_{23}'' \end{pmatrix}$	$\begin{pmatrix} \lambda_{13} + 2\lambda_{13}'' & 3\lambda_{13}'' \\ 3\lambda_{13}'' & \lambda_{13} + 2\lambda_{13}'' \end{pmatrix}$

TABLE XIV: Scattering matrices for two-scalar states.

- [1] CMS collaboration, S. Chatrchyan et al., *Observation of a New Boson at a Mass of 125 GeV with the CMS Experiment at the LHC*, *Phys. Lett. B* **716** (2012) 30–61, [[1207.7235](#)].
- [2] ATLAS collaboration, G. Aad et al., *Observation of a new particle in the search for the Standard Model Higgs boson with the ATLAS detector at the LHC*, *Phys. Lett. B* **716** (2012) 1–29, [[1207.7214](#)].
- [3] T. D. Lee, *A theory of spontaneous t violation*, *Phys. Rev. D* **8** (1973) 1226–1239.
- [4] E. A. Paschos, *Diagonal Neutral Currents*, *Phys. Rev. D* **15** (1977) 1966.
- [5] S. L. Glashow and S. Weinberg, *Natural conservation laws for neutral currents*, *Phys. Rev. D* **15** (1977) 1958.

- [6] N. G. Deshpande and E. Ma, *Pattern of Symmetry Breaking with Two Higgs Doublets*, *Phys. Rev. D* **18** (1978) 2574.
- [7] G. C. Branco, P. M. Ferreira, L. Lavoura, M. N. Rebelo, M. Sher and J. P. Silva, *Theory and phenomenology of two-higgs-doublet models*, *Phys. Rept.* **516** (2012) 1–102, [[1106.0034](#)].
- [8] J. F. Gunion and H. E. Haber, *Higgs bosons in supersymmetric models. i*, *Nucl. Phys. B* **272** (1986) 1–76.
- [9] J. A. Grifols and A. Mendez, *The WZH^\pm Coupling in $SU(2) \times U(1)$ Gauge Models*, *Phys. Rev. D* **22** (1980) 1725.
- [10] S. Kanemura, *Enhancement of loop-induced $h^\pm w^\mp z$ vertex in two higgs doublet models*, *Phys. Rev. D* **61** (2000) 095001, [[hep-ph/9710237](#)].
- [11] S. Kanemura, Y. Okada and E. Senaha, *Electroweak baryogenesis and quantum corrections to the triple higgs boson coupling*, *Phys. Lett. B* **606** (2005) 361–366, [[hep-ph/0411354](#)].
- [12] M. Aoki, S. Kanemura and K. Yagyu, *Probing the $h^\pm w^\mp z$ vertex in the two higgs doublet model at the lhc*, *Phys. Rev. D* **83** (2011) 075016, [[1102.3412](#)].
- [13] S. Kanemura, M. Kikuchi and K. Yagyu, *Radiative corrections to the higgs couplings in two higgs doublet models*, *Nucl. Phys. B* **896** (2015) 80–137, [[1502.07716](#)].
- [14] G. Abbas, D. Das and M. Patra, *Loop induced $H^\pm \rightarrow W^\pm Z$ decays in the aligned two-Higgs-doublet model*, *Phys. Rev. D* **98** (2018) 115013, [[1806.11035](#)].
- [15] N. Chakrabarty, I. Chakraborty and D. K. Ghosh, *Fingerprinting the contribution of colored scalars to the $H^+W^-Z(\gamma)$ vertex*, *Eur. Phys. J. C* **80** (2020) 1120, [[2003.01105](#)].
- [16] P. M. Ferreira and J. P. Silva, *Discrete and continuous symmetries in multi-higgs-doublet models*, *Phys. Rev. D* **78** (2008) 116007, [[0809.2788](#)].
- [17] A. C. B. Machado, J. C. Montero and V. Pleitez, *Three-higgs-doublet model with a4 symmetry*, *Phys. Lett. B* **697** (2011) 318–322, [[1011.5855](#)].
- [18] A. Aranda, C. Bonilla and J. L. Diaz-Cruz, *Three generations of higgses and the cyclic groups*, *Phys. Lett. B* **717** (2012) 248–251, [[1204.5558](#)].
- [19] I. P. Ivanov and E. Vdovin, *Discrete symmetries in the three-higgs-doublet model*, *Phys. Rev. D* **86** (2012) 095030, [[1206.7108](#)].
- [20] I. P. Ivanov and E. Vdovin, *Classification of finite reparametrization symmetry groups in the three-higgs-doublet model*, *Eur. Phys. J. C* **73** (2013) 2309, [[1210.6553](#)].
- [21] R. González Felipe, H. Serôdio and J. P. Silva, *Models with three higgs doublets in the triplet representations of a4 or s4*, *Phys. Rev. D* **87** (2013) 055010, [[1302.0861](#)].
- [22] R. Gonzalez Felipe, H. Serodio and J. P. Silva, *Neutrino masses and mixing in a4 models with three higgs doublets*, *Phys. Rev. D* **88** (2013) 015015, [[1304.3468](#)].
- [23] V. Keus, S. F. King and S. Moretti, *Three-higgs-doublet models: symmetries, potentials and higgs boson masses*, *JHEP* **01** (2014) 052, [[1310.8253](#)].
- [24] A. Aranda, C. Bonilla, F. de Anda, A. Delgado and J. Hernandez-Sanchez, *Higgs decay into two*

- photons from a 3hdm with flavor symmetry*, *Phys. Lett. B* **725** (2013) 97–100, [[1302.1060](#)].
- [25] I. P. Ivanov and C. C. Nishi, *Symmetry breaking patterns in 3hdm*, *JHEP* **01** (2015) 021, [[1410.6139](#)].
- [26] D. Das and U. K. Dey, *Analysis of an extended scalar sector with s3 symmetry*, *Phys. Rev. D* **89** (2014) 095025, [[1404.2491](#)].
- [27] M. Maniatis, D. Mehta and C. M. Reyes, *Stability and symmetry breaking in a three-Higgs-doublet model with lepton family symmetry $O(2)\otimes\mathbb{Z}_2$* , *Phys. Rev. D* **92** (2015) 035017, [[1503.05948](#)].
- [28] D. Das, *Implications Of The Higgs Discovery On Physics Beyond The Standard Model*. PhD thesis, University of Calcutta, 2015. [1511.02195](#).
- [29] S. Moretti and K. Yagyu, *Constraints on parameter space from perturbative unitarity in models with three scalar doublets*, *Phys. Rev. D* **91** (2015) 055022, [[1501.06544](#)].
- [30] N. Chakrabarty, *High-scale validity of a model with three higgs doublets*, *Phys. Rev. D* **93** (2016) 075025, [[1511.08137](#)].
- [31] M. Merchand and M. Sher, *Three doublet lepton-specific model*, *Phys. Rev. D* **95** (2017) 055004, [[1611.06887](#)].
- [32] D. Emmanuel-Costa, O. M. Ogreid, P. Osland and M. N. Rebelo, *Spontaneous symmetry breaking in the s3-symmetric scalar sector*, *JHEP* **02** (2016) 154, [[1601.04654](#)].
- [33] K. Yagyu, *Higgs boson couplings in multi-doublet models with natural flavour conservation*, *Phys. Lett. B* **763** (2016) 102–107, [[1609.04590](#)].
- [34] M. P. Bento, H. E. Haber, J. C. Romao and J. P. Silva, *Multi-higgs doublet models: physical parametrization, sum rules and unitarity bounds*, *JHEP* **11** (2017) 095, [[1708.09408](#)].
- [35] D. Emmanuel-Costa, J. I. Silva-Marcos and N. R. Agostinho, *Exploring the quark flavor puzzle within the three-higgs doublet model*, *Phys. Rev. D* **96** (2017) 073006, [[1705.09743](#)].
- [36] J. E. Camargo-Molina, T. Mandal, R. Pasechnik and J. Wessén, *Heavy charged scalars from cs-bar fusion: A generic search strategy applied to a 3hdm with $u(1) \times u(1)$ family symmetry*, *JHEP* **03** (2018) 024, [[1711.03551](#)].
- [37] S. Pramanick and A. Raychaudhuri, *Three-higgs-doublet model under a4 symmetry implies alignment*, *JHEP* **01** (2018) 011, [[1710.04433](#)].
- [38] I. de Medeiros Varzielas and I. P. Ivanov, *Recognizing symmetries in 3hdm in basis-independent way*, [1903.11110](#).
- [39] H. E. Logan, S. Moretti, D. Rojas-Ciofalo and M. Song, *CP violation from charged Higgs bosons in the three Higgs doublet model*, *JHEP* **07** (2021) 158, [[2012.08846](#)].
- [40] A. G. Akeroyd, H. E. Logan, S. Moretti, D. Rojas-Ciofalo, T. Shindou and M. Song, *CP-Violation in the 3-Higgs Doublet Model: CP-Asymmetries from Charged Higgs Bosons and Electric Dipole Moments*, [2111.11931](#).
- [41] A. Kuncinas, *Dark Matter and CP Violation in Some Symmetry-Constrained 3HDMs*. PhD thesis, Lisbon U., 6, 2025. [2506.08197](#).
- [42] A. Dey, J. Hernández-Sánchez, V. Keus, S. Moretti and T. Shindou, *On the CP properties of spin-0*

- dark matter*, *JHEP* **06** (2025) 206, [[2409.16360](#)].
- [43] V. Keus, L. Lewitt and J. Thomson-Cooke, *Electroweak phase transition enhanced by a CP-violating dark sector*, [2511.04636](#).
- [44] A. Kunčinas, P. Osland and M. N. Rebelo, *U(1)-charged Dark Matter in three-Higgs-doublet models*, *JHEP* **11** (2024) 086, [[2408.02728](#)].
- [45] N. Batra, B. Coleppa, A. Khanna, S. K. Rai and A. Sarkar, *Constraining the 3HDM parameter space using active learning*, *Phys. Rev. D* **112** (2025) 015011, [[2504.07489](#)].
- [46] S. Moretti, D. Rojas and K. Yagyu, *Enhancement of the $H^\pm W^\mp Z$ vertex in the three scalar doublet model*, *JHEP* **08** (2015) 116, [[1504.06432](#)].
- [47] M. Chakraborti, D. Das, M. Levy, S. Mukherjee and I. Saha, *Prospects for light charged scalars in a three-Higgs-doublet model with Z3 symmetry*, *Phys. Rev. D* **104** (2021) 075033, [[2104.08146](#)].
- [48] K. Fujikawa, *Xi-limiting process in spontaneously broken gauge theories*, *Phys. Rev. D* **7** (1973) 393–398.
- [49] M. Bace and N. D. Hari Dass, *Parity Violating Compton Amplitude in Unified Theories*, *Annals Phys.* **94** (1975) 349.
- [50] M. B. Gavela, G. Girardi, C. Malleville and P. Sorba, *A Nonlinear R(xi) Gauge Condition for the Electroweak SU(2) X U(1) Model*, *Nucl. Phys. B* **193** (1981) 257–268.
- [51] N. M. Monyonko and J. H. Reid, *ONE LOOP VACUUM POLARIZATION IN THE NONLINEAR R(XI) GAUGE*, *Phys. Rev. D* **32** (1985) 962–967.
- [52] J. M. Hernandez, M. A. Perez, G. Tavares-Velasco and J. J. Toscano, *Decay $Z \rightarrow neutrino anti-neutrino gamma$ in the standard model*, *Phys. Rev. D* **60** (1999) 013004, [[hep-ph/9903391](#)].
- [53] J. Hernandez-Sanchez, M. A. Perez, G. Tavares-Velasco and J. J. Toscano, *Decay $H^+ \rightarrow W^+ gamma$ in a nonlinear R(xi)-gauge*, *Phys. Rev. D* **69** (2004) 095008, [[hep-ph/0402284](#)].
- [54] G. 't Hooft and M. J. G. Veltman, *Scalar One Loop Integrals*, *Nucl. Phys. B* **153** (1979) 365–401.
- [55] T. Hahn and M. Perez-Victoria, *Automatized one loop calculations in four-dimensions and D-dimensions*, *Comput. Phys. Commun.* **118** (1999) 153–165, [[hep-ph/9807565](#)].
- [56] B. W. Lee, C. Quigg and H. B. Thacker, *Weak Interactions at Very High-Energies: The Role of the Higgs Boson Mass*, *Phys. Rev. D* **16** (1977) 1519.
- [57] J. M. Cornwall, D. N. Levin and G. Tiktopoulos, *Derivation of Gauge Invariance from High-Energy Unitarity Bounds on the s Matrix*, *Phys. Rev. D* **10** (1974) 1145.
- [58] M. P. Bento, J. C. Romão and J. P. Silva, *Unitarity bounds for all symmetry-constrained 3HDMs*, *JHEP* **08** (2022) 273, [[2204.13130](#)].
- [59] A. Djouadi, *The Anatomy of electro-weak symmetry breaking. I: The Higgs boson in the standard model*, *Phys. Rept.* **457** (2008) 1–216, [[hep-ph/0503172](#)].
- [60] A. Djouadi, *The Anatomy of electro-weak symmetry breaking. II. The Higgs bosons in the minimal supersymmetric model*, *Phys. Rept.* **459** (2008) 1–241, [[hep-ph/0503173](#)].
- [61] C. Collaboration, *Measurement of the Higgs boson inclusive and differential fiducial production cross*

- sections in the diphoton decay channel with pp collisions at $\text{sqrt}(s) = 13 \text{ TeV}$, *JHEP* **07** (2023) 091, [2208.12279].*
- [62] ATLAS collaboration, G. Aad et al., *Measurement of the properties of Higgs boson production at $\sqrt{s} = 13 \text{ TeV}$ in the $H \rightarrow \gamma\gamma$ channel using 139 fb^{-1} of pp collision data with the ATLAS experiment*, *JHEP* **07** (2023) 088, [2207.00348].
- [63] D. Toussaint, *Renormalization Effects From Superheavy Higgs Particles*, *Phys. Rev. D* **18** (1978) 1626.
- [64] M. E. Peskin and T. Takeuchi, *A New constraint on a strongly interacting Higgs sector*, *Phys. Rev. Lett.* **65** (1990) 964–967.
- [65] M. E. Peskin and T. Takeuchi, *Estimation of oblique electroweak corrections*, *Phys. Rev. D* **46** (1992) 381–409.
- [66] W. Grimus, L. Lavoura, O. M. Ogreid and P. Osland, *The Oblique parameters in multi-Higgs-doublet models*, *Nucl. Phys. B* **801** (2008) 81–96, [0802.4353].
- [67] M. Misiak, H. M. Asatrian, R. Boughezal, M. Czakon, T. Ewerth, A. Ferroglio et al., *Updated next-to-next-to-leading-order qcd predictions for the weak radiative b-meson decays*, *Phys. Rev. Lett.* **114** (Jun, 2015) 221801.
- [68] S. Moretti and J. Rathsman, *Charged Higgs bosons in three-Higgs-doublet models at the LHC*, *Eur. Phys. J. C* **75** (2015) 301, [1501.00900].
- [69] T. Bandyopadhyay, S. Chakraborty and D. Ghosh, *Probing three Higgs doublet models at the LHC*, *Phys. Rev. D* **95** (2017) 035021, [1607.06093].
- [70] A. Arhrrib, R. Benbrik, A. Jueid and G. Moultaka, *Collider phenomenology of a three-Higgs-doublet model*, *JHEP* **04** (2016) 136, [1507.03630].
- [71] V. Keus, S. F. King and S. Moretti, *Collider signals of inert scalars in three-Higgs-doublet models*, *Phys. Rev. D* **93** (2016) 075026, [1507.08433].
- [72] S. Ghosh, S. Moretti and R. Santos, *Charged scalar phenomenology in three-Higgs-doublet models at the LHC*, *Phys. Rev. D* **101** (2020) 055025, [2004.09823].
- [73] P. Boto, P. M. Ferreira, R. Santos and J. P. Silva, *LHC constraints on three-Higgs-doublet models*, *Phys. Rev. D* **104** (2021) 055023, [2106.03298].
- [74] A. G. Akeroyd and S. Moretti, *Production of charged Higgs bosons in three-Higgs-doublet models at e+e- colliders*, *Phys. Rev. D* **98** (2018) 035014, [1709.04551].
- [75] T. A. Chowdhury and A. Jueid, *Probing three-Higgs-doublet models at future muon colliders*, *Phys. Rev. D* **105** (2022) 075011, [2109.01942].
- [76] T. Mondal and S. Mukherjee, *Multi-Higgs signatures from three-Higgs-doublet models at the LHC*, *Phys. Rev. D* **106** (2022) 035016, [2203.08154].
- [77] B. Coleppa, A. Khanna and G. B. Krishna, *3HDM at the ILC*, **2506.24094**.
- [78] N. D. Christensen and C. Duhr, *FeynRules - Feynman rules made easy*, *Comput. Phys. Commun.* **180** (2009) 1614–1641, [0806.4194].
- [79] A. Alloul, N. D. Christensen, C. Degrande, C. Duhr and B. Fuks, *FeynRules 2.0 - A complete toolbox*

- for tree-level phenomenology, *Comput. Phys. Commun.* **185** (2014) 2250–2300, [1310.1921].*
- [80] C. Degrande, C. Duhr, B. Fuks, D. Grellscheid, O. Mattelaer and T. Reiter, *UFO - The Universal FeynRules Output, *Comput. Phys. Commun.* **183** (2012) 1201–1214, [1108.2040].*
- [81] R. Frederix, S. Frixione, V. Hirschi, D. Pagani, H. S. Shao and M. Zaro, *The automation of next-to-leading order electroweak calculations, *JHEP* **07** (2018) 185, [1804.10017].*